奈米生物感測粒子用於細胞內氧化壓力

即時偵測之發展及研究

Development of Intracellular Nanobiosensor for Oxidative Stress Detection

研 究 生：杜靜如　　　　　　　Student：Jing-Ru Tu

指導教授：袁俊傑 博士　　　　　Advisor：Dr. Chiun-Jye Yuan

國 立 交 通 大 學

生 物 科 技 系 所

碩 士 論 文

A Thesis
Submitted to Institute of Biological Science and Technology
National Chiao Tung University
In Partial Fulfillment of the Requirements
for the Degree of
Master
In
Biological Science and Technology

September 2009

Hsinchu, Taiwan, Republic of China

中華民國九十八年九月

Development of intracellular nanobiosensor for oxidative stress detection

Student: Jing-Ru Tu   Advisor: Dr. Chiun-Jye Yuan

Department of Biological Science and Technology
National Chiao Tung University

Abstract

Balance between oxidants and antioxidants is important to maintain normal cellular functions. Although the most oxidative events are carefully monitored and controlled by the natural defense systems of cells, sustained perturbation of this balance may result in oxidative stress. Oxidative stress-induced damages are usually key factors for aging and many disorders in human cell. In this study, a ratiometric optical PEBBLE (probes encapsulated by biologically localized embedding) nanosensor, which encapsulates catalase and two fluorescent dyes, Ru(II)-tris(4,7-diphenyl-1,10-phenanthroline) chloride ($[Ru(dpp)_3]^{2+}$) and Oregon Green 488-dextran was developed by sol-gel technology for the detection oxidative stress *in vivo*. The developed ratiometric optical PEBBLE nanosensor is spherical with an average size of 200±50 nm. The catalase encapsulated in the nanosensor is around 8U/mg nanoparticle. Catalase in nanosensor converts H_2O_2 to oxygen that quenches the fluorescence of $[Ru(dpp)_3]^{2+}$; whereas, the fluorescence of Oregon Green 488-dextran is unaffected, acting as a reference for ratiometric intensity measurement. The developed optical nanosensor exhibits potential for the real-time detection of oxidative stress in living cells.

奈米生物感測粒子用於細胞內氧化壓力即時偵測之發展及研究

學生: 杜靜如　　　　　　　　　　　　　　　　指導教授: 袁俊傑 博士

國立交通大學生物科技研究所碩士班

中文摘要

要維持生物細胞功能正常運作,細胞中的氧化劑及抗氧化劑的平衡作用是不可或缺的。一般來說,在自然的情況下,細胞會有相對應的防禦機制將氧化劑還原並維持體內氧化鈦平衡。當細胞因為自然因素或是外在因素致使細胞內產生額外的氧化劑,且防禦機制無法平衡時,過多的氧化劑與細胞中的各物質發生交互作用並造成氧化傷害,即氧化壓力(oxidative stress);關於氧化壓力及其所造城的傷害在近年來已經被證實與老化與多種疾病有關。在本文中,提出以光學比率測量原理為基礎的奈米生物感測粒子[PEBBLE (probes encapsulated by biologically localized embedding) nanosensor]。粒子中含有過氧化還原酵素－catalase (EC 1.11.1.6)以及兩種螢光染劑－Ru(II)-tris(4,7-diphenyl-1,10-phenanthroline) chloride ($[Ru(dpp)_3]^{2+}$) 和 Oregon Green 488-dextran。並使用 sol-gel 技術將上述物質包覆於例子中以用於偵測體內過氧化氫濃度。此光學比率測量奈米生物感測粒子粒子為圓球體,平均尺寸約為 200±50nm,並具有約 8U/mg 的 catalase 活性。Catalase 可以將細胞中造成氧化壓力的過氧化氫還原生成氧氣。同時,粒子中的$[Ru(dpp)_3]^{2+}$的螢光訊號會因為氧氣的存在而產生 quenching,造成螢光強度的改變;而相反的 Oregon Green 488-dextran 之螢光訊號則不受氧氣濃度影響,可作為測量的基準值,與$[Ru(dpp)_3]^{2+}$訊號相較以提供細胞內過氧化氫偵測資訊。

誌　謝

Index of Content

1. Introduction

1.1. Oxidative stress

Living in oxygenated environment, the balance between oxidants and antioxidants is important to maintain normal cell functions. As a consequence of aerobic metabolism, oxidants are constantly formed in organisms. These oxidants are usually oxygen molecules containing one or more unpaired electrons, which are called reactive oxygen species (ROS). ROS occur endogenously and exogenously by metal-catalyzed enzyme reactions, neutrophils and macrophages during inflammation and the leakage of mitochondrial electron transport reactions [1]. While ROS are generated, the cellular natural defense system will act in concert to detoxify oxidants. The overall oxidant level is strictly regulated by sophisticated enzymatic and non-enzymatic systems, including catalase (CAT), superoxide dismutase (SOD), glutathione peroxidase (GPx) and vitamins A, C and E, to maintain the physiological homeostasis.

However, the intrinsic balance between oxidants and anti-oxidants can be influenced by many environmental stresses. For example, oxidants can be generated during irradiation of UV light, X-rays, and γ- rays. Toxins and drugs can also elevate the oxidants in cells. Under these conditions, the level of oxidants quickly elevates and exceeds that of antioxidant, rising up the oxidative level within cells. The highly active oxidants would easily react with many biomolecules, such as proteins, nucleic acids and lipids, to give

oxidative damages.

Oxidative stress is generally defined as a disturbance in the oxidant-antioxidant balance, resulting in potential oxidative damages [3]. The presence of ROS can be an indicator of oxidative stress. Studies in last decades have found that oxidative stress resulting damages are accumulative [2]. Accumulation of oxidative damages to DNA, to proteins and to lipids in cells are closely correlated with aging, aging related diseases, cardiovascular diseases, neurodegenerative disorders and cancers [4-5]. Besides, ROS also act as specific signaling molecules under both pathophysiological and physiological conditions with certain boundaries [2].

1.2. Properties of ROS
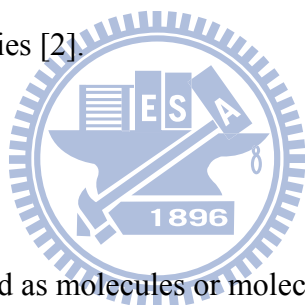
Free radicals can be defined as molecules or molecular fragments containing one or more unpaired electrons in atomic or molecular orbitals. The unpaired electrons usually give a considerable degree of reactivity to the free radicals [6-7]. ROS are radical derivatives of oxygen and the most prominent free radicals in biological systems. ROS encompass a wide variety of oxygen-containing free radicals including superoxide anion ($O_2^-\bullet$), hydrogen peroxide (H_2O_2), singlet oxygen ($^1O_2$), hydroxyl radical ($\bullet OH$), and peroxyl radical ($ROO\bullet$). Although H_2O_2 is not a free radical, it may easily break down into harmful hydroxyl radical ($\bullet OH$) with the presence of metal ions. Most ROS are extremely unstable, short-lived, and charged, causing great damages to the sites where they are

produced. In contrast, hydrogen peroxide is rather stable, long-lived and uncharged thus

diffusible between membranes [2] to give random damages within the cell.

1.3. Sources of ROS

ROS can be produced from both endogenous and exogenous substances (Figure 1).

Mitochondria, cytochrome P450, and peroxisomes are potential endogenous sources in

inflammatory cells for ROS generation [1].
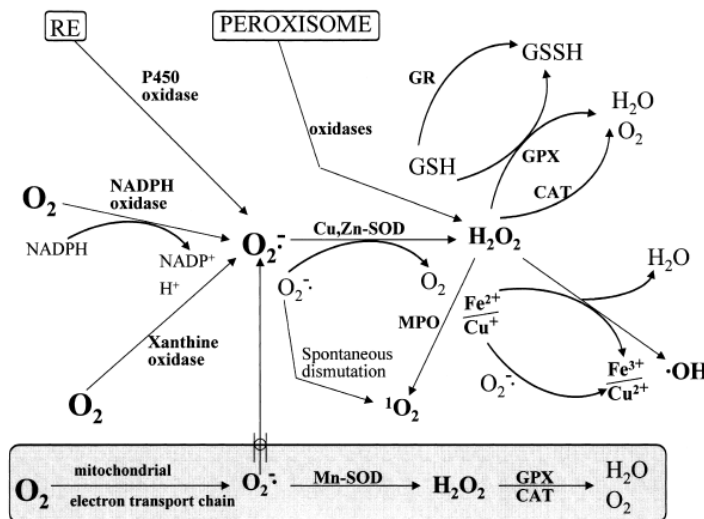
Figure.1. Endogenous ROS sources and main defense mechanisms [9].

In aerobic cells, the mitochondrial electron transport chain is one of essential sources

for ROS [8]. The electron transport chain in the mitochondrial inner membrane plays an

important role in the generation of ATP. During the process of oxidative phosphorylation,

electrons from electron donors, e.g., NADH and $FADH_2$, pass along the electron transport

chain and promote the generation of proton (H^+) gradient cross the mitochondrial inner

membrane. Ultimately, electrons are accepted by dioxygen (O_2), resulting in the formation

of H_2O. However, a portion of electrons may leak from electron transport chain and forms

superoxide anions ($O_2^-\bullet$) by interacting with dissolved dioxygen. Under physiological

conditions, superoxides are constantly produced from both Complexes I (NADH

dehydrogenase) and III (ubiquinone–cytochrome c reductase) of the electron transport

chain [7].

Evidence indicates that around 1–2% dioxygen molecules are converted into

superoxide anions ($O_2^-\bullet$) instead of contributing to the reduction of oxygen to water [1-2,

6-8]. The generated superoxide anions ($O_2^-\bullet$) are then consumed by Mn-superoxide

dismutase (MnSOD) to produce hydrogen peroxide [9]. Compare to the strong negative

charged superoxide anions ($O_2^-\bullet$), hydrogen peroxide is permitted to diffuse through

mitochondrial membranes. Once hydrogen peroxide meets transition metal ions, such iron,

cupper and cobalt ions, in the environment, hydroxyl radical ($\bullet OH$) quickly forms due to

Fenton reaction (Eq. 1) [1,10].

$$M^{n+} + H_2O_2 \;\rightarrow\; M^{(n+1)} + \bullet OH + OH^- \qquad (\, M = Cu^{2+},\, Fe^{2+},\, Ti^{4+},\, Co^{3+}) \quad (Eq.\ 1)$$

Under the stress, an excess of superoxide induces the release of iron ions from

iron-containing proteins, such as [4Fe–4S] cluster containing enzymes of the

dehydratase-lyase family [7]. The released Fe^{2+} then triggers the conversion of hydrogen

peroxide to the highly reactive hydroxyl radical ($\bullet OH$) by Fenton reaction [1, 6]. Reactive

hydroxyl radicals are also generated by Haber-Weiss reaction (Eq. 2). in the presence of

superoxide and hydrogen peroxide. In this reaction, Fe^{3+} is reduced by superoxide to yield

Fe^{2+} and oxygen ($Fe^{3+} + O_2^-\bullet \rightarrow Fe^{2+} + O_2$) [1, 7]. The hydroxyl radical ($\bullet OH$) is highly

reactive with a half-life in aqueous solution of less than 1 ns. Thus when produced *in vivo*

it reacts close to its site of formation.

$$O_2^-\bullet + H_2O_2 \ \rightarrow \ O_2 + \bullet OH + OH^- \qquad \text{(Eq. 2)}$$
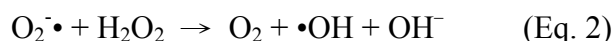
The phase I cytochrome P-450 is the terminal component of the monoxygenase

system found within the endoplasmatic reticulum (ER) of most mammalian cells. The main

role of cytochrome P-450 is to convert foreign toxic compounds into less toxic products in

the presence of dioxygen [11]. This enzyme also participates in removing or inactivating

xenobiotic compounds by hydroxylation. In addition, monoocygenase is also involved in

steroidogenesis. During the oxidation and hydroxylation reactions electrons may 'leak' into

surrounding environment, in which they may be uptaken by dioxygen molecules and form

superoxide radicals ($O_2^-\bullet$) [6].

Microsomes and peroxisomes are also the sources of ROS. Microsomes are

responsible for the 80% H_2O_2 produced in tissues with hyperoxia [6]. Peroxisomes are

known to produce H_2O_2, but not $O_2^-\bullet$ under physiologic conditions [6]. Peroxisomal

Oxidation of fatty acids in peroxisomes was recognized as one of potentially sources for

H_2O_2 production after prolonged starvation [1, 6-7]. Although peroxisome is ubiquitously

distributed in all organs, liver is the primary organ for the production of H_2O_2 by

peroxisomes. Neutrophils generate and release superoxide radical ($O_2^-•$) by nicotine

adenine dinucleotide phosphate (NAD(P)H) oxidase to induce the destruction of bacteria.

On the other hand, the nonphagocytic NAD(P)H oxidases produce superoxide at a level

only 1–10% to that produced in neutrophiles. Superoxide radicals are thought to play a role

in the intracellular signaling pathways [7].

1.4. Influences of ROS

It has been estimated that one human cell is exposed to approximately 10^5 oxidative

hits a day from hydroxyl radicals and other such species [6]. Although all types of

bio-molecules may be attacked by free radicals, lipid is probably the most sensitive one.

Cell membranes are rich sources of polyunsaturated fatty acids, which are readily attacked

by ROS. Lipid peroxidation involves very destructive chain reactions that cause damage on

the structure of membrane directly or the damage of other cell components indirectly by

producing reactive aldehydes. Lipid peroxidation has been implicated to be involved in a

wide range of tissue injures and diseases, such as atherosclerosis [4].

Random oxidative damages of proteins may not give very destructive consequences to

cell function unless the damages are very extensive and/or accumulative. Proteins may be

damaged by the transition metal ion that binds at their specific site(s). The reaction

between transition metal ion and hydrogen peroxide generates harmful hydroxyl radical

(•OH) that further causes oxidative damages of proteins [4].

ROS can attack bases or deoxyribose of DNA to produce damaged bases or strand

break. Alternatively, the intermediates generated from the oxidation of lipid or protein

molecules by oxygen radicals may react with DNA to form adducts. Attempt to replicate

this damaged DNA sequence leads to mutation and/or apoptosis [12]. Permanent

modification of genetic material resulting from these oxidative damages represents the first

step of carcinogenesis.

Several lines of evidence suggest that oxidative stress-induced damages are

indiscriminate and accumulative. Damages accumulated in DNAs, proteins and lipids are

potential keys for the development of aging and age-related diseases, such as cancers,

vascular diseases [13], arthritis and neurodegenerative diseases. Oxidative stress is also

found to be responsible for dysfunction or death of neuronal cells that contributes to the

pathogenesis of several diseases [18], such as amyotrophic lateral sclerosis [14],

Parkinson's disease [15] and Alzheimer's disease [16-17].

1.5. Methods of intracellular detection for oxidative stress

Oxidative stress and its bringing effects are thought to be playing an essential role in

the pathogenesis of many diseases and disorders. ROS was shown to be the indicator of

oxidative stress. Thus, the detection of concentration and distribution of ROS in cell is

important to understand the relation between oxidative damage and cell responses.

However, it is difficult to track ROS within biological systems due to their short life time

and high reactivity to almost all substances. For example, the half life of hydroxyl radical

($\cdot$OH), is about 1 ns. Conventionally, the detection of ROS relies on the measurement of

products or intermediates of free radical oxidative reactions, which are also transitory in

nature [4]. Common ways to detect ROS in cells including lipid peroxidation assays, image

analysis based on ROS-specific fluorescence dyes and electron spin resonance (ESR).

A suitable detection method for ROS is necessary to allow scientist to elucidate the

role of certain types of free radicals in oxidative stress. Oxidation reactions could be a

wide-ranged and prolonged process due to the characteristics of oxidative damages are

usually random and accumulative. Therefore, real-time monitoring ROS in cell may help to

elucidate the true role of oxidative stress. Several criteria are required for the development

of sensors for the detection of ROS, including fast detection, high sensitivity, good

reproducibility and miniaturization [19]. The detection of ROS has to be fast in order to

follow actual changes, in particular the interplay with other reactive species. Rather low

concentrations have to be analyzed since the range under physiological conditions covers

the nano- and micromolar concentration level. The sensor configuration should be stable

under repeated radical bursts in order to be reusable several times. The effect of

miniaturization of the sensor elements for the spatially resolved detection and high

selectivity of the sensor signal for the reactive species is under investigation.

1.5.1. Lipid peroxidation assay

Lipid peroxidation is one of the most widely used indicators of oxidant/free radical formation *in vitro* and *in vivo*. Potent oxidants, such as hydroxyl radical, peroxyl radicals, nitrogen dioxide, and higher oxidation states of heme and hemoproteins (ferryl heme), are capable of initiating peroxidation of polyunsaturated fatty acids. The appearance of oxidative stress can be determined by detecting of the lipid oxidation product, F_2-isoprostanes (IsoP). Detection of oxidative stress by lipid peroxidation assay exhibits many advantages, including low interferences, noninvasiveness and proportional to radicals [20-21]. However, low sensitivity, low reliability and required other quantitative method for the quantification of oxidized lipids are the major drawbacks of this approach. Moreover, this approach reflects oxidative stress condition indirectly without knowing the level of ROS in cells [20].

1.5.2. Fluorescence probes used for intracellular detection of ROS

Fluorescence dye is commonly used in the measurement of ROS because of its high sensitivity, simplicity in data collection, and high spatial resolution in conjugating with microscopic imaging techniques [21]. Some fluorescent probes have been developed for the detection of ROS, such as dichlorodihydrofluorescein and its numerous derivatives. Dichlorodihydrofluorescein (2′,7′-dichlorodihydrofluorescein diacetate [2′,7′-dichlorofluorescein diacetate; H_2DCFDA or DCFHDA]) is a membrane permeable

fluorescence dye for hydrogen peroxide and hydroxyl radical [21-22]. When DCFHDA

passively enters cells, the cellular esterases cleaves DCFHDA into

2′,7′-dichlorodihydrofluorescein (DCFH$_2$). Generated DCFH$_2$ can be oxidized by

peroxidases, cytochrome c and Fe^{2+} to form 2′,7′-dichlorofluorescein (DCF, $\lambda_{excitation}$=498

nm; $\lambda_{emission}$=522 nm) in the presence of hydrogen peroxide. The generated DCF is then

accumulated and trapped in cells. A flow cytometer can de used to detect the fluorescence

signal of DFC, which is proportional to the concentration of hydrogen peroxide in cells.

However, it has been found that some DCFHDAs are quite sensitive to ambient O$_2$

levels, and tends to be oxidized by illumination light alone. In addition to hydrogen

peroxide, DCFH$_2$ can also be oxidized by a variety of ROS and RNS (reactive nitrogen

species, that contain nitrogen with one or more unpaired electrons), causing a noise during

the detection. Moreover, high degree of cellular leakage of fluorescence dyes remains

common to all of the fluorescein-derived dyes, which brings difficulties to long-term

monitoring of ROS [23]. At present, fluorescent probes based on boronate are the only

contrast agents that can detect hydrogen peroxide with high specificity at physiologic

concentrations. However, their potential for *in vivo* imaging is limited because of low

tissue penetrating ability [24].

1.5.3. Electron paramagnetic resonance (EPR) probes used for intracellular ROS detection

Electron spin resonance (ESR) spectroscopy, also known as electron paramagnetic resonance (EPR), is at present the only analytic approach that permits the direct detection of free radicals. This technique provides information about the magnetic properties of unpaired electrons and their molecular environment by detecting energy differences between unpaired electrons at different spin states under an applied magnetic field [20]. A "spin-trap" is used to stabilize the free radicals, which is very short-lived and unstable, during the detection. The spin trapping reagent reacts with highly reactive radicals to produce relatively longer-lived carbon adduct than that of the primary reactive free radicals. The stable radical adducts are detectable by their characteristic features in EPR spectra [25].

With spin trapping reagent, ESR spectroscopy is capable of detecting the unstable free radical-derived species produced during oxidative and inflammatory injury. However, the spin-trapping reagent is lack of specificity and the secondary adduct might be metabolized by tissue though time. In addition, the cost of ESR is high, making this technique less attractive than other detection methods for the *in vivo* determination of free radicals [20].

1.6. Applications of nanotechnology in biological researches

The concept of nanotechnology was first touched at 1960s and then began to enter into

mainstream of physical sciences and engineering from 1980s [26]. With the capability of

controlling matters within nano-scale ($<10^{-9}$ m), nanotechnology has been applied to

manufacture materials and devices in a variety of applications, including medicine,

electronics, cellular imaging and clinical diagnosis. While living cells and organisms are

formed with various biological molecules of nano-scale, the application of nanotechnology

in the researches of life science and biomedicine is inevitable [27].

Recently, various nanodevices (e.g., nanoparticles, nanotubes, and nanowires) were

developed and employed in the biological and biomedical researches. The dimension of the

fabricated nanodevies can be controlled by predictable manufacture method [28].

Nowadays, nanoparticles have been widely used in development and delivery of imaging

contrast agents, anti-cancer drugs, enzymes and diagnosis probes in animal model [29,

31-33]. Nanoparticles can be fabricated by various materials, such as metal oxides (e.g.,

iron oxide, silica oxide and titanium oxide), carbon nanostructure, gold and silica. Among

these materials, silica nanoparticles have been widely used for chemical mechanical

polishing and as additives to drugs, cosmetics, printer toners, varnishes, and food [30].

1.6.1. Synthesis of nanoparticles by sol-gel process

The fabrication of nanoparticles sol-gel technology involves the concept of

polycondensation, which gives three-dimension network-like matrix with pores (10~1000

nm in size) within the structure. Thus porous sol-gel is ideal for doping with biomolecules.

The flexible process also allows the product to be tailored in size, shape and porosity by controlling reaction condition. In addition, the silica particle is optical transportable, high purity and chemically inert, thus makes it an ideal material to biological applications.

The history of sol-gel science could be trace to about 40 years ago. Stöber and coworkers [34] reported a sol-gel process that hydrolyzes TEOS in the presence of basic catalyst and produce powders with controlled morphology and size [35]. *Sols* are dispersions of colloidal particles in a liquid where *colloids* are solid particles with diameters of 1-100 nm. A *gel* is an interconnected, rigid network with pores of submicrometer dimensions and polymeric chains [35]. Therefore, a sol-gel process includes gel formation from colloid particles in sol.

A typical sol-gel process involves 4 steps: (i) hydrolysis, (ii) condensation (iii) gelation (iv) aging. At the hydrolysis step, a silica alkoxide precursor, commonly use tetraethoxysilane (TEOS) and tetramethoxysilane (TMOS), is added to a mixture of ethanol containing base or acid (such as aqueous ammonium hydroxide or hydrogen chloride) as hydrolyzing catalyst. The precursor is then hydrolyzed into hydroxy derivatives (e.g., silicicacids, hydroxometallates and hydroxysilanes) [36] (Eq. 3).

$$Si(OR)_4 + nH_2O \rightarrow (HO)_n\text{-}Si(OR)_{4\text{-}n} + nROH \qquad R= C_2H_5 \text{ or } CH_3 \qquad (Eq. 3)$$
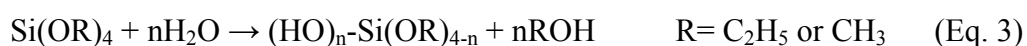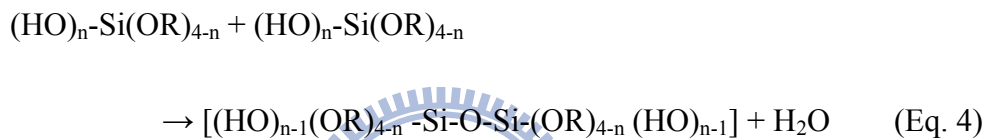
Hydrolysis condition greatly affects the hydrolysis rate of silica alkoxide precursor. With acidic electrophilic mechanism, the stronger acid uses in the hydrolysis, the faster

hydrolysis rate occurs. The hydrolysis can also be catalyzed by basic neuclophilic

mechanism. However, the hydrolysis rate is no only influenced by the concentration of

base but also the steric effect of the alkoxyl group of silica alkoxide precursor.

Once hydroxyl derivatives formed, the condensation reaction between two hydroxyl

groups of hydrosylated silica occurs and forms Si-O-Si linkage (siloxane bond). As the

reaction goes further, a polycondensation occurs to form an extensive linkage between

hydroxyl groups of hydrolyzed hydrosylated tetrahedral silica (Eq. 4 and Eq. 5) [35].

$$(HO)_n\text{-}Si(OR)_{4\text{-}n} + (HO)_n\text{-}Si(OR)_{4\text{-}n}$$

$$\rightarrow [(HO)_{n\text{-}1}(OR)_{4\text{-}n}\text{ -}Si\text{-}O\text{-}Si\text{-}(OR)_{4\text{-}n}\,(HO)_{n\text{-}1}] + H_2O \qquad (Eq.\ 4)$$

Polycondensation:

(Eq. 5)
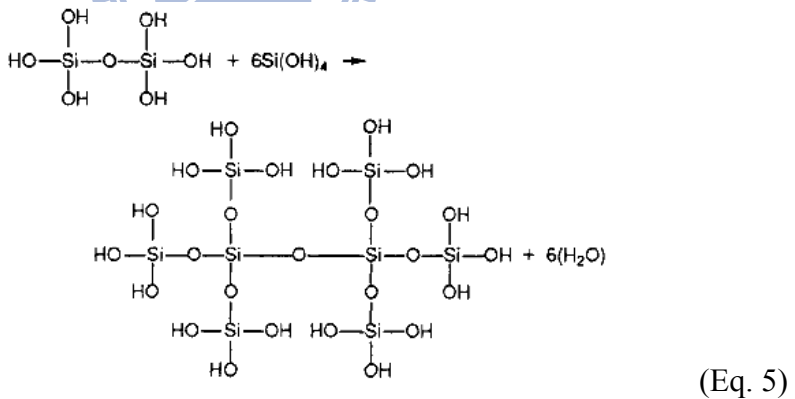
Polycondensation reaction eventually leads to gelation (Eq. 5), causing the formation

of a three-dimensional cross-linked polymer. The size and structure (e.g. density or

porosity) of the silica particles are dominated by R ratio, a ration of $[H_2O]$ to $[Si(OR)_4]$, pH

value and reaction rate in the early steps. During the polymerization, trapping small

molecules into the porous of the silica particles is possible.

Aging of a gel is a time-dependent process, in which condensation remains for a period of time (hours to days) [37]. It further strengthens the structure of sol-gel matrix. Finally, the drying process removes the liquid in the space of sol-gel matrix. When liquid is removed under the hypercritical condition (critical point drying), the highly porous aerogel can be obtained. Drying the gel by thermal evaporation leads to pore-collapse and bulk shrinkage. Under this condition, the product becomes xerogel, which is poor in porosity, but high in hardness. In addition, the process can also be tailored to form different kinds of product such as thin film, rod, particle and electrode coating.

1.6.2. Entrapment of enzyme in silica sol-gel

The development of sol–gel derived biomaterials start in the 1990, Braun and coworkers successfully entrapped enzyme in sol-gel matrix [38]. Ever since, lots of works have described the entrapment of a wide variety of biological species, including enzymes, antibodies, regulatory proteins, membrane-bound proteins and nucleic acids [39]. Several studies have demonstrated that the entrapped enzymes are still functional for the applications of kinetic study, biological analysis and biocatalyzation [32, 38-39]].

An ideal enzyme entrapping matrix should retain enzymes tightly inside a mechanically stable, chemically inert hydrophilic porous matrix. The silica sol-gel derived matrix exhibits an unparalleled optical property, which is ideal for optical signal detection (e.g., fluorescence or absorbance). Silica sol-gel also exhibits high chemical stability and

physical durability that can protect enzymes from denaturation by environmental factors,

such as pH and temperature. The modification of silica sol-gel is easy through flexible

sol-gel process by adding polymerizable or nonpolymerizable organic substituents to form

an organic/inorganic hyubid material (Ormosils). In addition, the pore size and pore

distribution of silica sol-gel are tuneable that allows analytes diffuse into and product

diffuse out of the matrix easily without disturbing the entrapped enzymes [32, 36, 39].

A general enzyme sol-gel entrapping process involves hydrolysis and

polycondensation stages as described previously. The sol-gel precursors (e.g. silica

alkoxides) are hydrolyzed, at least partially, in the mixture to form aqueous sol. At this

stage, additives, such as organic polymers, protein stabilizers, drying control additives,

templating agents, redox species or fillers that modify silica matrix, can be added and

mixed with the precursor in the presence of catalyst, either acid or base [39]. Subsequently,

the polycondensation reaction occurs to form cross-linked silicate structure to entrap

protein molecules. The gelation is then performed for a period to time based on the

requirement of applications. Finally, water and ethanol are removed by drying under the

4°C to obtain the enzyme-encapsulated silica sol-gel.

### 1.6.3. Probes encapsulated by biologically localized embedding (PEBBLEs)

The intracellular detection becomes more and more important for the understanding

of biological functions and cellular responses. Therefore, developing a suitable nano-scaled

intracellular probe seems necessary to fulfill these tasks. The probes should be narrowed

down in scale and non-toxic in order to offer an intracellular detection with least physical

or chemical disturbances to cell. Therefore, measurement of chemical and physical

parameters with negligible physical disturbance and high spatial resolution becomes an

important issue of the intracellular environment measurement [40].

Development of bionanotechnology opens a new horizon for the detection of specific

chemical species within cells directly. In 1998, Clark and co-works [41] described a

stand-alone nano-sphere optical sensor, which is consisting of several key components

necessary for the intracellular detection. The sensor, know as PEBBLEs (probe

encapsulated by biologically localized embedding), was reported to be capable of detecting

some chemical changes occurred in cells. The concept of PEBBLE was demonstrated to be

feasible for the fabrication of optical nanosensors for intracellular detection (Table 1).

A typical PEBBLEs is now give a clear definition as an optical nano-sensor (20-200

nm), which encapsulates an analyte-specific dye (indicator dye) and a reference dye within

a biologically inert matrix. Polyacrylamide, polydecylmethacrylate (PDMA), metal oxide,

and organically modified silicates (Ormosils) are known matrices to be used in the

fabrication PEBBLEs. The confinement of the indicator dyes enables the differentiation of

nano-optode locations from those of auto fluorescence centers in cell and also makes the

simultaneous observation of analytes possible [42]. The small size and inert characteristic

of PEBBLEs provide a distinct sensing mechanism for intracellular environment and can possibly avoid the chemical interference and cytotoxicity to cell [43]. Furthermore, PEBBLE optical nanosensors offer several advantages over conventional ways for real-time detection of intracellular substances, including proventing loading dye from degrading, protecting intracellular environment from toxic dyes, easy detection and quantification [49]. Compare to loading free dyes into cell, the inert matrix of PEBBLEs protects the intracellular environment from potentially toxic effects of the sensing dyes. The matrix can also protect the sensing dyes from potential interferences from the cellular components, such as non-specific binding proteins and organelles. PEBBLE is small in size, giving negligible physical perturbation to cell. Nanosensors have not being reported to be selective sequestrated into cellular compartments, leak from cell or even be pumped out of cells. Finally, PEBBLE provides a ratiometric measurement by the embedded multiple dyes.
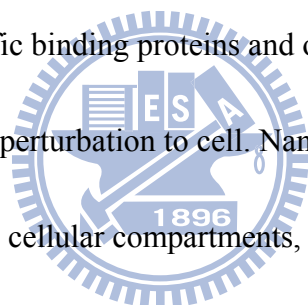
2. Objective

Accumulating oxidative damages caused by oxidative stress is harmful to cells. Since ROS are responsible of oxidative injuries of oxidative stress, a real-time detection of ROS distribution and concentration change is essential to understand how cell responses against oxidative stress. Among various ROS, hydrogen peroxide is an uncharged molecule with a relatively lower reactivity and longer life time than other free radicals. These characteristics allow hydrogen peroxide to diffuse through membranes in cell and bring oxidative damages all over the cell.

In order to detect the generation of hydrogen peroxide real-time, we designed a sol-gel glass-based PEBBLE to detect intracellular hydrogen peroxide. The PEBBLE will encapsulate a catalase (EC 1.11.1.6) and two fluorescent dyes by sol-gel process. Oregon Green 488-dextran® (FITC derivatives and connected with dextran) and Ru(II)-tris(4,7-diphenyl-1,10-phenanthroline) chloride ($[Ru(dpp)_3]^{2+}$), two fluorescent dyes, are chosen to be entrapped in the PEBBLE. While catalase specifically consume H_2O_2 to produce oxygen, resulting in a fluorescent quenching effect on the oxygen-sensitive dye, $[Ru(dpp)_3]^{2+}$. The other fluorescence dye, Oregon Green 488-dextran® is an oxygen-insensitive dye, will give an unaffected fluorescence emission signal as reference [46, 47]. A ratiometric measurement can be made by collecting the signal of $[Ru(dpp)_3]^{2+}$ and Oregon Green 488-dextran®.

The detection principle is summarized in the schematic diagram bellow.
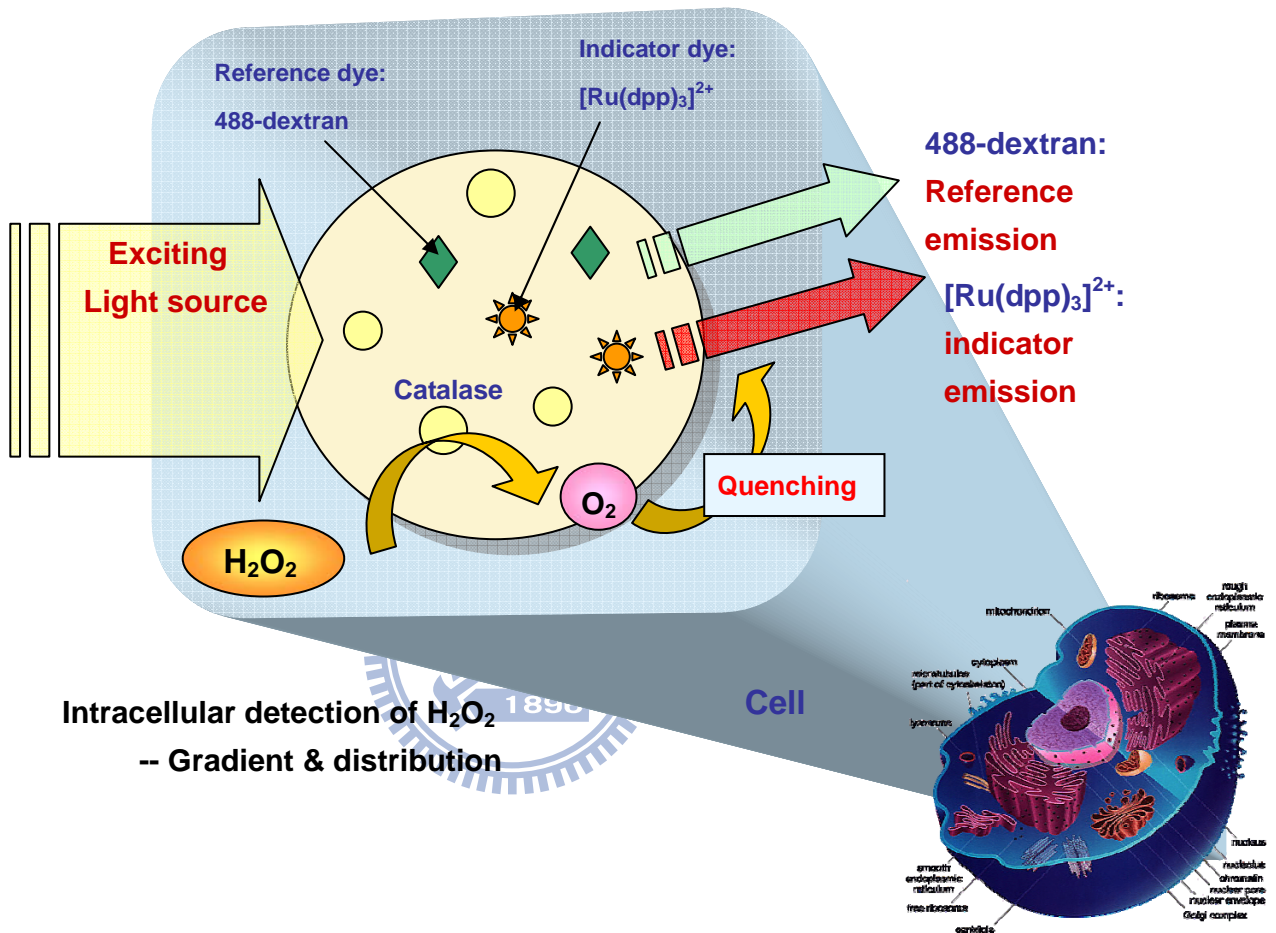
Catalase reduces H_2O_2 in the environment and forms Oxygen.

(Catalase + $2H_2O_2 \rightarrow 2H_2O + O_2$)
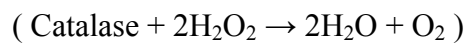
The emission signal of entrpped $[Ru(dpp)_3]^{2+}$ quenches (result in intensity decrease)
by the out coming oxygen.

Comparing quenched signal with Oregon Green 488-dextran[®] (stable emission,
oxygen insensitive) to get detection message.

3. Material and methods

3.1. Materials

Catalase (EC 1.11.1.6, from bovine liver, lyophilized powder, 2000-5000 units/mg protein; bCAT), horseradish peroxidase (HRP type VI, EC1.11.1.7, lyophilized powder, 275 units/mg solid), tetraethyl orthosilicate (TEOS, reagent grade, 98%), bovine serum albumin (BSA, lyophilized powder), MTT (3-(4-5-Dimethylthiazol-2-yl)-2,5-diphenyltetrazolium bromide) and 2,2'-azino-bis (3-ethylbenzthiazoline-6-sulphonic acid) (ABTS) were purchased from Sigma-Aldrich. Polyethylene glycol 6000 (PEG, MW 6000), ammonium hydroxide (28%) and hydrogen peroxide (H_2O_2, 30%) were obtained from SHOWA. Catalase (EC 1.11.1.6, from *Corynebacterium glutamicum*, solution, ~500000 U/mL; cgCAT) and indicator fluorescent dye, Ru(II)-tris(4,7-diphenyl-1,10-phenanthroline) chloride ([Ru(dpp)$_3$]$^{2+}$, were purchased from Fluka. The oxygen-insensitive dye, Oregon Green 488-Dextran® (MW 10000) was purchased from Molecular Probe. Ethanol (95%) is obtained from TTL, Taiwan. In addition, water used to prepare solutions was autoclaved double distilled water. DMEM (Dulbecco modified Eagle's minimal essential medium), FBS (fetal bovine serum), penicillin, and streptomycin were purchased from GIBCO Life Technology.

3.2. Preparation of enzyme entrapped sol-gel PEBBLEs

The hydrogen peroxide sensitive PEBBLEs, bCAT-Ru/488-PEBBLE and

cgCAT-Ru/488-PEBBLE, that contain fluorescent dyes, $[Ru(dpp)_3]^{2+}$, Oregon Green

488-Dextran® and catalase were prepared as described previously with modification [46].

Briefly, 2.5g poly(ethylene glycol) (PEG, MW 6000 monomethyl ether) was first dissolved

in a mixture containing 6 mL ethanol (95%), 25μL Oregon Green 488-dextran (MW 10

000) (stock 0.1 mM in H_2O), 200μL $[Ru(dpp)_3]^{2+}$ (stock 0.4 mM in 95% ethanol), and 4.2

mL 28 wt % ammonia water for 30 minutes or until the solution became transparent and

viscous. Ammonia is served as a catalyst, while water acts as one of the reactants.

The enzyme stock solution was prepared separately by dissolving enzyme in double

distilled water (ddH$_2$O). The specific activity of HRP was determined as described in

Section 3.3 and diluted to 1000 units /mL solution. Various amounts (0.1, 0.08, 0.05, 0.03

and 0.01 g) of catalase from bovine liver (powder, 2000-5000 units/g) were dissolved in 1

mL water to obtained the stock solutions. Whereas, the catalase stock solution from

Corynebacterium glutamicum (~500000 Units/mL buffered solution containing ~30%

glycerol and 10% ethanol) was prepared by diluting 10 μL, 30 μL or 50 μL original

enzyme solution in water containing 2.5 mg BSA to give a final volume of 1 mL. The

enzyme stock solution (1 mL each) was mixed with 0.5 mL TEOS to make an

enzyme/TEOS sol. The enzyme/TEOS sol was then added into a vigorously stirred PEG

stock solution that was prepared previously by micropipette to initiate the hydrolysis and

condensation reaction. About 1/3 of enzyme/TEOS sol was added at a time. The stirring

continued for at least 1 h to allow the gelation to proceed thoroughly. To prevent

fluorescent dye from photobleaching, the reaction is performed in the dark.

The whole solution was then transferred to enppendorf tubes and centrifuged at

13,000 rpm for 9 min. The supernatant was discarded to remove the unreacted monomers,

such as PEG, ammonia, and dye molecules. The pelleted PEBBLEs were washed by

suspending in the autoclaved PBS buffer and centrifuged at 13,000 rpm for 3 min. Remove

and discard supernatant carefully after centrifugation. Repeat washing process at least three

times. Finally, PEBBLEs was stored in PBS buffer under 4°C. The control nanoparticles

were also produced by the same process without enzymes and dyes.

3.3. Activity assay of HRP and HRP-entrapped particles

Activity of HRP and HRP-entrapped particles was performed with a conventional

peroxidase assay by using ABTS and hydrogen peroxide as subtracts [50]. A standard 1 mL

activity assay solution contains ?? units HRP, 0.5 mM ABTS (ammonium salt) (Boehringer

Mannheim) and 3 mM H_2O_2 in 100 mM sodium acetate buffer (pH of 5.5) . ABTS is

oxidized by HRP in the presence of H_2O_2 to form an oxidized form, which exhibits an

absorbance at 405 nm (dark green in color). The activity was determined colorimetrically

by using a UV–Vis spectrophotometer (HITACHI U-3010) to record the variation of

absorbance with time in the presence of oxidized ABTS. The extinction coefficient of

oxidized ABTS (ε_{ABTS}) at 405 nm is 36.8 mM^{-1} cm^{-1} (at 25˚C, pH 5.5) for following

calculations. One unit HRP is defined as oxidizing 1 μmole of ABTS within one min. at 25

˚C and pH 5.5.

Particles were sonicated for 10 minutes in PBS buffer to prevent aggregation before

activity assay. The activity of HRP-entrapped silica nanoparticle was then measured by

using the same assay process as that of free HRP. The background absorption of

HRP-entrapped silica nanoparticle was subtracted from the total absorption. There is no

obvious background absorption when the particles used is in the range of 0.01-0.1 mg.

3.4. Activity assay of catalase and catalase-entrapped PEBBLEs

Catalase activity was determined by recording absorbance change at 240 nm of 10

mM hydrogen peroxide in 50 mM potassium phosphate buffer (pH 7.0) on a UV-Vis

spectrometer (HITACHI U- 3010). The total volume of reaction mixture is 1 mL. The

detecting principle was based on the conversion of hydrogen peroxide and generating H_2O

and O_2. Thus, one unit of catalase is defined as decomposing 1 μmole H_2O_2 per minute at

pH 7.0 and 25°C. The molar absorption coefficient for H_2O_2 (ε_{H2O2}) is 39.4 M^{-1} cm^{-1}.

The catalase entrapped-PEBBLEs were sonicated for 10 min. in PBS to prevent

aggregation prior to activity assay. The activity of catalase entrapped-PEBBLEs was

determined as the same assay process as that of free catalase. Catalase

entrapped-PEBBLEs at low concentration give stable absorbance background at 240 nm.

Background absorbance is determined by adding catalase entrapped-PEBBLEs into

potassium phosphate buffer as reference before catalase activity assay. However, when

catalase entrapped-PEBBLE activity is low, longer incubation is needed to obtain a

significant change in the absorbance of H_2O_2. Therefore, a calibration curve was conducted

by using a catalase/HRP coupled enzyme assay system to avoid the existence of high

background due to the addition of large amount of catalase entrapped-PEBBLE particles.

Catalase was diluted by PBS buffer in a concentration of 3.5, 4, 4.5 and 6 units in 10

μL. Each assay solution contained 50 mM potassium phosphate buffer and 10 mM H_2O_2

with a final volume of 1 mL. The reaction mixture was allowed to stand at room

temperature for 30 min. An obvious oxygen bubbles can be observed in tube during

reaction. After incubation, the remaining H_2O_2 in the tube was further detected by a HRP

assay. A portion of the above catalase reaction solution (100 μL) was added to HRP assay

solution (100 mM sodium acetate buffer, pH 5, containing 0.5 mM ABTS and 10 units of

HRP) with final volume of 1mL. The assay mixture was allowed to stand at room

temperature for 5 min. The absorbance of oxidized ABTS was determined on a UV–Vis

spectrophotometer (HITACHI U-3010) at 405 nm. Each catalase activity point was

repeated for at lease three times. PEBBLEs exhibit no obvious background in following

HRP assay at 405 nm.

3.5. Scanning Electron Microscope (SEM) Imaging

PEBBLEs were dispersed in water and sonicated for 20 min. to prevent aggregation. Place 2 μL of the PEBBLE suspension on the small piece of silica wafer and dried gradually in an anti-humidity cabinet. The sample was then sputter coated with platinum (12V, 90 sec.), and the SEM images were taken on the Thermal Field Emission Scanning Electron Microscope (JEOL, JSM-6500F).

3.6. Fluorescent spectroscopy spectrum of PEBBLEs and fluorescent calibration

PEBBLEs (10 mg) were dispersed in 1 mL water and sonicated for 20 min. to prevent aggregation. In each 10 mg PEBBLEs/H_2O suspension solution 1 mL of various concentrations of hydrogen peroxide was added to make the final concentrations of 0.1, 0.5, 1, 5, 10 and 20 mM. The final volume of reaction mixture is 2 mL. The mixture was then mixed thoroughly in a 3-mL cuvette and incubated at room temperature for 3 minute, followed by wave scanning fluorescence detection on the HITACHI F-4500 with exciting wavelength of 488 nm. The emission scanning range was between 500 and 750 nm. The obtained emission intensity (ransom light units; RLU) of $[Ru(dpp)_3]^{2+}$ at 607 nm was normalized with the emission intensity units of Oregon Green 488-Dextran at 524 nm. The normalized value from control was defined as 100%.

3.7. Cell culture

The human cervical carcinoma cell line (HeLa) was maintained in DMEM (Dulbecco modified Eagle's minimal essential medium) containing 10% FBS, 100 units/mL penicillin, and 100 μg/mL streptomycin (GIBCO Life Technology). Cells were incubated in a humidified 37˚C incubation chamber containing 5% CO_2. Cells were subcultured for every 2-3 days.

3.8. Cell viability test

Cell viability was measured by the MTT (3-(4-5-Dimethylthiazol-2-yl)-2,5 -diphenyltetrazolium bromide) assay. HeLa cells were seeded on 24-well culture plates with 2×10^4 cells in 500 μL culture medium per well and put in humidified 37˚C incubation chamber for 24 hour prior to assay. Afterward, each well was treated with 100 μg, 200 μg, 300 μg and 400 μg of the sonicated catalase-entrapped PEBBLEs and control (silica-PEG only) particles in PBS for 24 and 48 h. At the end of incubation, cultural medium was removed and cells were washed once with pre-wormed PBS, followed by incubating with 500 μL MTT solution (0.5 mM in culture medium) in a 37 ˚C incubation chamber containing 5% CO_2 for 3 h.

The produced blue-purple formazan in each well was solubilized with 600 μL acidic isopropanol (0.1 N HCl in absolute isopropanol). The absorbance soluble formazan was quantified at 540 nm using the UV–Vis spectrophotometer (HITACHI U-3010). The

viability of the treated group was expressed as the percentage of control group (added no

PEBBLEs but PBS buffer only) which was assumed to be 100%.

3.9. Cell images

The location of the PEBBLEs in HeLa cells was monitored using an inverted

fluorescence microscope. The HeLa cells (4×10^5 cells/well) were cultured in a 6-well

cultural dish with a sterilized cover glass with in 2 mL culture medium and put in

humidified 37°C incubation chamber for 24 h. Each well is then incubated with the

PEBBLEs in PBS. After incubation at 37°C for 24 h, cells were fixed with 4%

paraformaldehyde in pH 7.4 PBS at room temperature for 20 min, followed by PBS wash

for 4 times and monitoring under the inverted fluorescent microscope (Leica DMIL
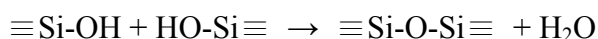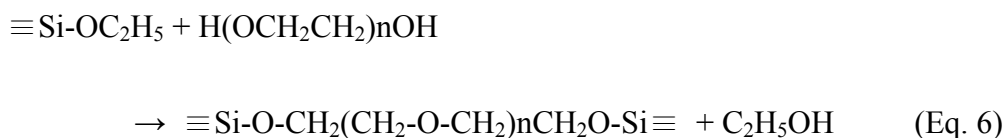
model).
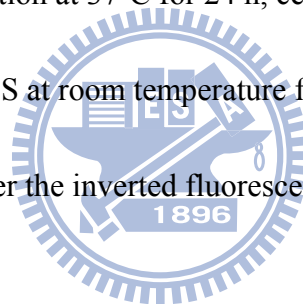
4. Results and discussion

4.1. PEBBLEs formation

Silica is well known for its advantages in biological-friendly chemical properties, optical clarity, porosity and controllable sol-gel fabricated process. These advantages make silica as a potential matrix for biological applications. However, such material can be brittle, may undergo cracking owing to hydration stresses, and, in some cases, can block the accessibility of analytes to the entrapped biomolecules [39]. Silica particles derived from conventional Stöber method usually have the size in micrometer scale due to aggregations between colloid particles during condensation stage in sol-gel process. Additionally, drying process may also cause irreversible aggregation of silica particles and forms precipitation by inter-particle hydrogen bonding. An improvement in the preparation of silica nanoparticle was reported by Xu and colleagues [46] by adding the organic additive, polyethylene glycol (PEG MW 6000), in the TEOS precursor to modify the chemical and physical properties silica nanoparticles (e.g., size and morphology) [51].

Polyethylene glycol (PEG , $\text{HO}\diagdown\diagup_\text{O}\diagdown\diagup_n\text{OH}$, $H(OCH_2CH_2)_nOH$) is a biocompatible linear polymer with low toxicity. It is also biodegradable. The hydroxyl group at the two end of the structure would participate in condensation reaction between silica alkoxide precursor and PEG during the sol-gel process (Eq. 6).

$$\equiv\!Si\text{-}OH + HO\text{-}Si\!\equiv\ \rightarrow\ \equiv\!Si\text{-}O\text{-}Si\!\equiv\ + H_2O$$

$$\equiv Si\text{-}OC_2H_5 + H(OCH_2CH_2)nOH$$

$$\rightarrow \ \equiv Si\text{-}O\text{-}CH_2(CH_2\text{-}O\text{-}CH_2)nCH_2O\text{-}Si\equiv \ + C_2H_5OH \qquad (Eq.\ 6)$$

PEG was demonstrated to be anchored on the surface of the silica particles by

covalent bonds (Si-O bond) between the silica alkoxide precursor $((HO)_n\text{-}Si(OR)_{4\text{-}n})$ and

PEG [46, 51-53]. Possibly, the PEG chain may extend from the surface of particles into the

solution. Thus, in a solution, the aggregation among the nanoparticles can be prevented by

the repulsion force and solvation layer of the PEG surface moiety [52]. In addition, PEG

also exhibit an effect on the formation of silica nanoparticles of colloidal size during

condensation through the formation of both covalent bonds with silicon alkoxide and

hydrogen bonds with residual silanol groups in the structure silica nanoparticle [54]. This

postulation was demonstrated by the observation under the thermal field emission scanning

electron microscopy (SEM) (Fig.1a,and 1b) The silica nanoparticles coated with PEG

exhibited smaller size (400-500 nm in diameter) than that of silica nanoparticles without

coating (700-800 nm in diameter). Both types of nanoparticles are smooth and

spherical-shaped. This result indicates that PEG modification do not alter the morphology

of nanoparticles.

PEG coating also affects the behavior of silica nanoparticle in aqueous solution. The

generated PEG-coated PEBBLEs took a shorter time (around 10 min.) to be resuspended in

a buffer by sonication than that of silica nanoparticles without PGE coating. It took around

30 min. to allow silica nanoparticles to be resuspended in a buffer by sonication. Therefore, PEG coating on the surface of the silica nanoparticles acts as a steric stabilizer to prevent silica nanoparticles from forming aggregates by hydrogen bonds.

4.2. HRP entrapment in silica-PEG particle

Two enzymes, HRP (EC1.11.1.7) and catalase (EC 1.11.1.6), were used as models to study protein entrapment in PEBBLEs for H_2O_2 detection. HRP is a widely used enzyme in biological applications because of its small size (~44 kDa), high temperature resistance and less expensive. Furthermore, the activity of HRP is well defined and easily to be determined. For decades, ABTS was used as a common chromogen for HRP to quantify hydrogen peroxide. This assay protocol allows us to easily determine the initial rates in the enzymatic reaction by a spectrometer. Recent study also demonstrated that HRP using ABTS as substrate can be readily applied for the determination of the activity of enzyme encapsulated in silica glass matrix [56].

The specific activity of HRP-entrapped in silica particle coated with PEG (silica-PEG-HRP NP) was summarized in Table 2. The activity of silica-PEG-HRP NP was 0.3 units/mg particles with a diameter of about 500 nm in diameter. This result shows that HRP is able to be entrapped in the nanoparticles and retain all or part of its original activity. However, the morphology of silica-PEG-HRP NP was irregular and the size was also diverse (Fig. 2). Some agglomerate could also be found in the SEM images. HRP

adsorption to the precursor during sol-gel process could be the reason.

4.3. Catalase entrapment in PEBBLEs particle

Catalase is a tetrameric heme-containing enzyme with a molecular of around 240 kDa. It is largely but not exclusively, localized in peroxisomes, where many H_2O_2-producing enzymes reside in. As a protective mechanism for oxidative stress, catalase exhibits a extremely high turnover numbers for H_2O_2, allowing a quick removal of H_2O_2 to avoid its diffusion to other parts of the cell. Interestingly, catalase degrades H_2O_2 without consuming cellular reducing equivalents, providing cells with an energy efficient mechanism to remove H_2O_2. It has been proposed that catalase may play an essential role in regulating the homeostasis of H_2O_2 in cells. In practical, catalase was used widely for removing H_2O_2 in manufactured food and other industrial usage.

In this study, different amount of catalase was mixed with TEOS/PEG sol to study the encapsulating efficiency of the adapted sol-gel process. The activity of encapsulated catalase in silica nanoparticles in each preparation was summarized in Table 2. As shown in Figure 3, increasing amount of catalase leads to obvious particle aggregation and amorphous morphology with a smaller particle size than that of without catalase. When the TEOS/PEG sol contains 10, 30, 50, 80, or 100 mg catalase in the synthesized silica-PEG particles exhibited a size of 150±10, 130±50, 100±50, 80±50, and 70±50 nm (size distribution become diverse when the amount of adding catalase is increased), respectively.

37

This result indicates that the size of generated nanoparticles reduced aroung 100-300 nm in the presence of catalase compared to the particles without protein entrapped. Based on the effect of catalase on the size of fabricated silica-PEG nanoparticles, we chose a reaction mixture containing TEOS/PEG and 50 mg catalase for the fabrication of catalase-entrapped PEBBLEs.

The catalase-entrapped PEBBLE containing two fluorescence dye, $[Ru(dpp)_3]^{2+}$ and Oregon Green 488-Dextran[®], (bCAT-Ru/488-PEBBLE) for intracellular hydrogen peroxide detection was prepared. $[Ru(dpp)_3]^{2+}$ and Oregon Green 488-Dextran[®] were mixed with PEG prior to the addition of TEOS/(50 mg) catalase (bovine liver) sol. The specific activity of bCAT-Ru/488-PEBBLE was assay and determined. The resulting activity was 0.03 units/mg particles. The reduction of catalase activity probably due to protein denature by the strong base (e.g., NH_4OH in sol-gel process) and ethanol in the reaction. To overcome these problems, a thermal stable and pH insensitive catalase may be needed.

Catalase from *Corynebacterium glutamicum* (*C. Glutamicum.*) was reported to exhibit a better thermal and pH resistance than that from bovine liver [57-58]. Thus catalase from *C. Glutamicum* was then used to prepare catalase-entrapped silica/PEG nanoparticles. In a total reacting mixture, different amounts of catalase form *C. Glutamicum* was added into TEOS/PEG sol for the fabrication of catalase-entrapped silica/PEG nanoparticles. As shown in Figure 6, the obtained nanoparticles are less aggregate and exhibits a spherical

morphology with an average size within 400 nm. The specific activity of

catalase-entrapped silica/PEG nanoparticles was 20~138 units/mg nanoparticles dependent

on the amount of catalase used in the sol-gel process (Table 2). In addition, the catalase

from *C.Glutamicum* was kept in a buffered solution with 30% glycerol, which might help

to stabilize catralsae under the basic condition [59].

4.4. Fluorescence calibration of sol-gel PEBBLEs

Organic fluorescent ruthenium complex, $[Ru(dpp)_3]^{2+}$, a luminescence dyes, is used as

an indicator dye in many applications and is readily quenched by oxygen [28]. It exhibits

many characteristics, such as photostable, long excited-state life time (5.3 μs), high

luminescence quantum yield (~30%) and long life time, The reference dye, Oregon Green

488-Dextran®, was normally used in neuronal tracing. It is a stable FITC derivative, giving

a strong emission peak at 524 nm. The covalent-bonded dextran molecule formed a large

backbone which could be greatly trapped within the particle matrix. The hydroxyl groups

on the dextran may also participate in condensation reaction to give more rigid interaction

of the particle. In the sol-gel process, the well dispersed, hydrophobic organic ruthenium

complex dye and Oregon Green 488-Dextran® could be trapped in the porous oxide gel

matrix when gelation occurs, the dye molecules are, forming an organic–inorganic

nanomaterial [60]. It has been indicated that two dyes exhibited an excellent stability inside

the sol-gel matrix [46]. No leakage of dyes was observed in the developed

catalase-entrapped PEBBLE, i.e., bCAT-Ru/488-PEBBLE, suggesting that even small size

dyes could not diffuse through the porous structure into the surrounding environment. PEG

coat in the catalase-entrapped PEBBLE may act as an organic shell to prevent leakage of

dyes from inner core.

The fluorescence emission calibration curve of bCAT-Ru/488-PEBBLE was shown in

Figure 7. Two distinct emission peaks at 607nm ($[Ru(dpp)_3]^{2+}$) and 524nm (Oregon Green

488-Dextran$^®$) were observed. Unless mentioned, the catalase encapsulated in the

PEBBLE is from bovine liver. However, the emission peak of Oregon Green 488-Dextran$^®$

(524 nm) is relatively weak compared to the peak of $[Ru(dpp)_3]^{2+}$ at 607 nm. The reason

for this reason is unknown. Interestingly, when adding various concentrations of H_2O_2 into

the bCAT-Ru/488-PEBBLE suspension solution the fluorescent peak at 607 nm quenched

in a dose-dependent manner; whereas, the fluorescent peak at 524 nm was almost

unchanged (Figure 7). This result suggests that the developed bCAT-Ru/488-PEBBLE is

capable of responding to H_2O_2 and providing an appropriate signal.

The fluorescent spectrum of the cgCAT-Ru/488-PEBBLE with catalase from

C.Glutamicum was also studied (Figure 8). However, the encapsulated Oregon Green

488-Dextran$^®$ exhibited a extremely strong fluorescent emission at 524 nm. In comparison,

the emission peak at 607 nm is relatively weak, indicating that two dyes were not

entrapped evenly within the nanoparticles. It is possible that the catalase composition from

different commercial resources the affect the encapsulation efficiency of two dyes in the

TEOS/PEG nanoparticles. Therefore, an extra protein (e.g., BSA) was added along with

catalase in the TEOS sol during the preparation of cgCAT/BSA-Ru/488-PEBBLE. Figure 8

showed that when BSA was added, the intensity of Oregon Green 488-Dextran[®]

fluorescent peak decreased; while the fluorescent peak of $[Ru(dpp)_3]^{2+}$ increased. When 10

mg BSA along with catalase was added in the preparation mixture during sol-gel process

the fluorescent response of Oregon Green 488-Dextran[®] was almost disappeared. This

result suggests that the encapsulation of Oregon Green 488-Dextran[®] in silica/PEG matrix

may be interfered with BSA. In contrast, BSA may facilitate the entrapment of

$[Ru(dpp)_3]^{2+}$ dye. It is postulated that $[Ru(dpp)_3]^{2+}$ dye may be absorbed on the surface of

proteins via charge interactions (positively charged of $[Ru(dpp)_3]^{2+}$). In this study, the

cgCAT/BSA-Ru/488-PEBBLE was fabricated by adding a TEOS sol containing 30 μL

catalase from *C.Glutamicum* and 2.5 mg BSA into the PEG/ethanol/ammonium solution

containing both $Ru(dpp)_3]^{2+}$ and Oregon Green 488-Dextran[®] fluorescent dyes for

subsequent condensation and gelation reactions.

The fluorescent calibration curve of cgCAT/BSA-Ru/488-PEBBLE was performed by

adding various concentrations of H_2O_2 (0~10 mM). As showed in Figure 9, the quenching

of the fluorescent peak of $[Ru(dpp)_3]^{2+}$ at 607nm, was inversely proportion to the

concentration of $[H_2O_2]$. This result suggests that the developed

cgCAT/BSA-Ru/488-PEBBLE is capable of responding to H_2O_2 and providing an appropriate signal.

4.5. Particle morphology

The morphology of silica nanoparticles may be changed by the entrapping molecules that added during the sol-gel reaction as observed in SEM images (Figures 1-4, 6, 10). The Reaction compositions are summarized in Table 2. The presence of PEG may reduce the size of the generated particles (Figure 1b). This is similar to the effect of Oregon Green 488-Dextran® (Figure 1d). On the other hand, when $[Ru(dpp)_3]^{2+}$ or proteins (e.g., catalase and HRP) was added, morphology and the size of particles were unchanged (Figures 1c, 2, and 3). These results suggest that substances sue in sol-gel reaction, including acidic/basic and charged residues, may influence the mechanism and rates of alkoxysilane hydrolysis and condensation. Any molecule with charge or polarity may form electrostatic, hydrophobic, and/or H-bonding between molecules and silica alkoxides, resulting in interfacial templates that control the formation of developing polysilicate/polysiloxane colloids to generate branching pattern, functionality, growth, topology, and aggregation [61].

Therefore, when enzyme is added into the process and disperses in the solvent. Enzyme may adsorb onto the silica surface in a variety of orientations, associate with different functional groups at the silica–solvent interface, partition into a specific phase

within a nanocomposite material, or even aggregate if the protein is present at a high enough concentration [39].

4.6. Cell uptake and cytotoxicity of PEBBLEs

The cgCAT/BSA-Ru/488-PEBBLEs particles were incubated with HeLa cell for a day and then uptake rate was discussed through fluorescent microscope images (Figures 11a-c). As the green fluorescence of the Oregon Green 488-Dextran® (524nm) showed in Figure 11b, indicated that the fluorescence signal of the cgCAT/BSA-Ru/488-PEBBLEs is successfully entrapped in the silica-PEG matrix and ready to be detected by fluorescent microscope. The comparison is also made by using silica-PEG particle (Figure 11d-f), since there was no fluorescence signals, the fluorescence signal were contributed by the Oregon Green 488-Dextran® (524nm) is confirmed.

The uptake and distribution of the PEBBLEs particles were observed by the overlaid image of Figure11a and 11b in 11c. The particles are occurred in the overlapping region of the cell, and the background was very clean with no particles. Since wash process was repeated for 4 times, it indicated that the particles were located inside the cell and the particles were able to enter the cell through an endocytosis process.

Meanwhile, the cell viability test by MTT assay was also under processing. 2×10^4 HeLa cell in 24-well plate was treated with 200-1000μg/mL silica-PEG particles and cgCAT/BSA-Ru/488-PEBBLEs respectively for 48h. Preliminary results show that 80%

cell viability of cgCAT/BSA-Ru/488-PEBBLEs and 40% of silica-PEG particles under

600μg/mL. This result indicated that toxicity would not come from fluorescence dyes and

proteins within particles.

Since cgCAT/BSA-Ru/488-PEBBLEs and silica-PEG particles are different in size

(200-300nm for cgCAT/BSA-Ru/488-PEBBLEs and 400-500nm for silica-PEG particles)

and morphology (both spherical in shape but roughed surface for

cgCAT/BSA-Ru/488-PEBBLEs comparing to silica-PEG particles) result in different

surface area. A report of silica-based nanoparticle toxicology in 2009 indicted that the

toxicity of silica nanoparticle is strongly depends on the particle size, concentration and

metabolic activity of the cells [62].

On the other hand, cgCAT/BSA-Ru/488-PEBBLEs contain catalase, BSA and

fluorescence dyes within particle matrix which may brings structural and functional

discrepancies. The presence of catalase reduces hydrogen peroxides as an oxidative stress

defender while giving detection in cell.

5. Conclusion

In this work, a nano-sized particle with silica matrix coated with PEG was fabricated. The particles were synthesized using a modified Stöber method incorporating PEG monomethyl work as a steric stabilizer to reduce aggregation between the particles while narrow down particle diameter. The particle is also entrapped catalase, $[Ru(dpp)_3]^{2+}$ and Oregon Green 488-dextran with retaining enzyme activity. The combination of the catalase and dyes enabled a ratiometric fluorescent determination of hydrogen peroxide in vitro. We also find that the amount of protein in sol-gel compositions are closely concerned with the particle morphology and entrapping rate to fluorescence dyes.

Continued investigations in the future will focus on in vitro measurement. The cell uptake rate by endocytosis and cytotoxicity will be study next. Meanwhile, further improve the detecting limit is also important to let the CAT-PEBBLEs to be able to give real-time hydrogen peroxide detection within physiological concentration (from μM to mM).

In summary, we report details the preparation of enzyme-entrapped PEBBLE nanosensors and their characterization. The same fabrication method can be applied to produce photodynamic nanoplatforms for various applications.

Table 1. The reported PEBBLEs sensors

Matrix material	Analytes	Encapsulated components Indicator dye & reference dye / Other components	
Polyacrylamide	pH Ca^{2+}	Five varieties of pH-sensitive sensors and three different calcium-selective sensors & Sulforhodamine 101	[44] [45]
PDMA[1]	K$^+$	BME-44 ionophore (optically silent ionophores to fluorescence-based sensing by using ion-exchange)	[45]
Ormosil Silica-PEG	O$_2$	[Ru(dpp)$_3$]Cl$_2$ & Oregon Green 488-dextran	[46]
Polyacrylamide	Glucose	(Ru[dpp(SO$_3$Na)$_2$]$_3$)Cl$_2$ & Oregon Green 488-dextran or Texas Red-dextran / Glucose oxidase (GOx)	[40]
Ormosil Silica-PTMS[2]	O$_2$	platinum(II) octaethylporphine & 3,3′-dioctadecyloxacarbocyanine perchlorate platinum (II) octaethylporphine ketone & octaethylporphine	[47]
Polyacrylamide	Cu^{2+} Cu$^+$	The red fluorescent protein (DsRed) & Alexa Fluor 488 dextran	[48]

[1] PDMA: Polydecylmethacrylate; [2] PTMS: Phenyltrimethoxysilane

Table 2. Conditions for the synthesis of PEBBLEs

Reaction Composition

Containing EtOH 50%, NH4OH 10%, TEOS 4%, H2O 36% and PEG 6000 2.5g[1] for each reaction.

	Enzymes			Protein (mg)	Fluorescence Dye (mM)		Description Specific activity (units/mg)
	HRP (mg)	Catalase *B.L* [2] (mg)	Catalase *C.G.* [3] (µL)	BSA	$[Ru(dpp)_3]^{2+}$	Oregon Green 488-Dextran®	
Sample 1 Fig.1a	-	-	-	-	-	-	Silica only -
Sample 2 Fig. 1b	-	-	-	-	-	-	Silica-PEG -
Sample 3 Fig. 2	3.6	-	-	-	-	-	Silica-PEG-HRP 0.3units/mg
Sample 4 Fig. 3a-e	-	10-100[4]	-	-	-	-	Silica-PEG-CAT -
Sample 5 Fig. 4	-	50	-	-	0.4	0.1	bCAT/BSA-Ru/488 -PEBBLE 0.03units/mg
Sample 6 Fig. 6	-	-	10 30 50	-	-	-	Silica-PEG-CAT 20units/mg 90units/mg 138units/mg
Sample 7 Fig. 9a	-	-	30	2.5	0.8	0.05	cgCAT/BSA-Ru/488 -PEBBLE 7.8units/mg
Sample 8 Fig. 9b	-	-	30	10.0	0.8	0.05	cgCAT/BSA-Ru/488 -PEBBLE <0.5units/mg

[1] PEG 6000 was not contained in sample 1

[2] Catalase from *Bovine Liver*, powder, 2950units/mg

[3] Catalase from *Corynebacterium glutamicum*, solution, 1500units/µL

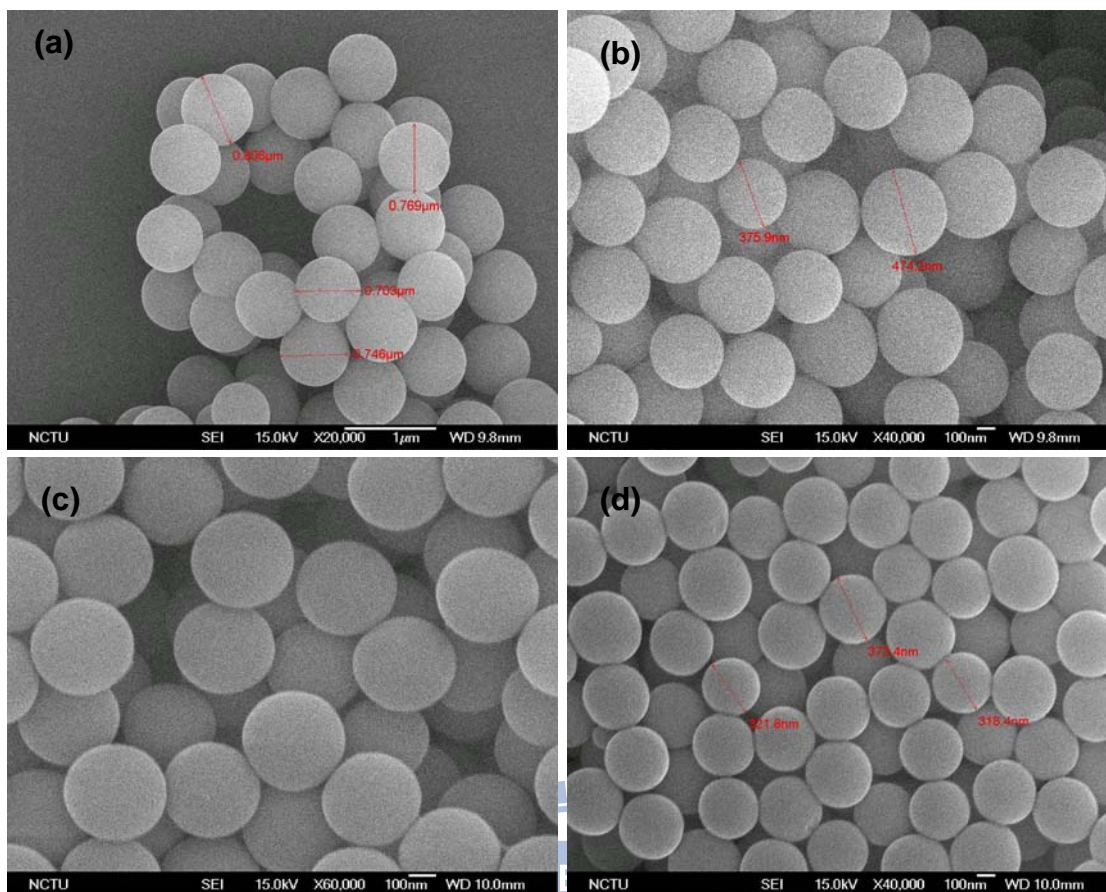[4] 10mg, 30mg, 50mg, 80mg and 100mg of Catalase from *Bovine Liver* were added

Figure 1. SEM images of Silica and Silica-PEG particles

(a) Particle synthesized by silica only, exhibiting a size of 700-800 nm in diameter. (b)

Particles generated by silica-PEG exhibit a size distribution of 400-500 nm in diameter. (c)

Silica-PEG-[Ru(dpp)$_3$]$^{2+}$ particles exhibit a size of 700-800 nm in diameter. (d)

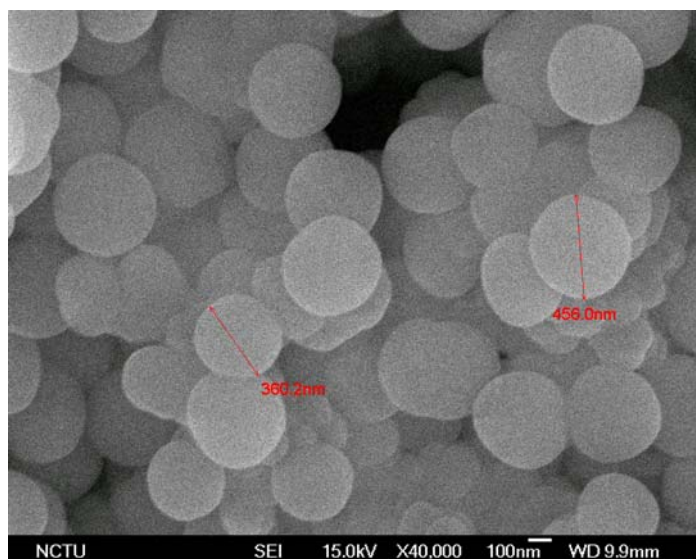Silica-PEG- Oregon Green 488-Dextran® particles exhibit a size of 300-400 nm in

diameter.

Figure 2. SEM images of Silica-PEG-HRP particles

HRP was used as an enzyme model to fabricate enzyme-entrapped particles. As the image

shows, the morphology of Silica-PEG-HRP was irregular and the diameter was also

diverse from 200 to 500 nm in diameter. Some agglomerate could also be found in the

SEM images. Particle was calibrated by the activity assay and the specific activity was 0.3

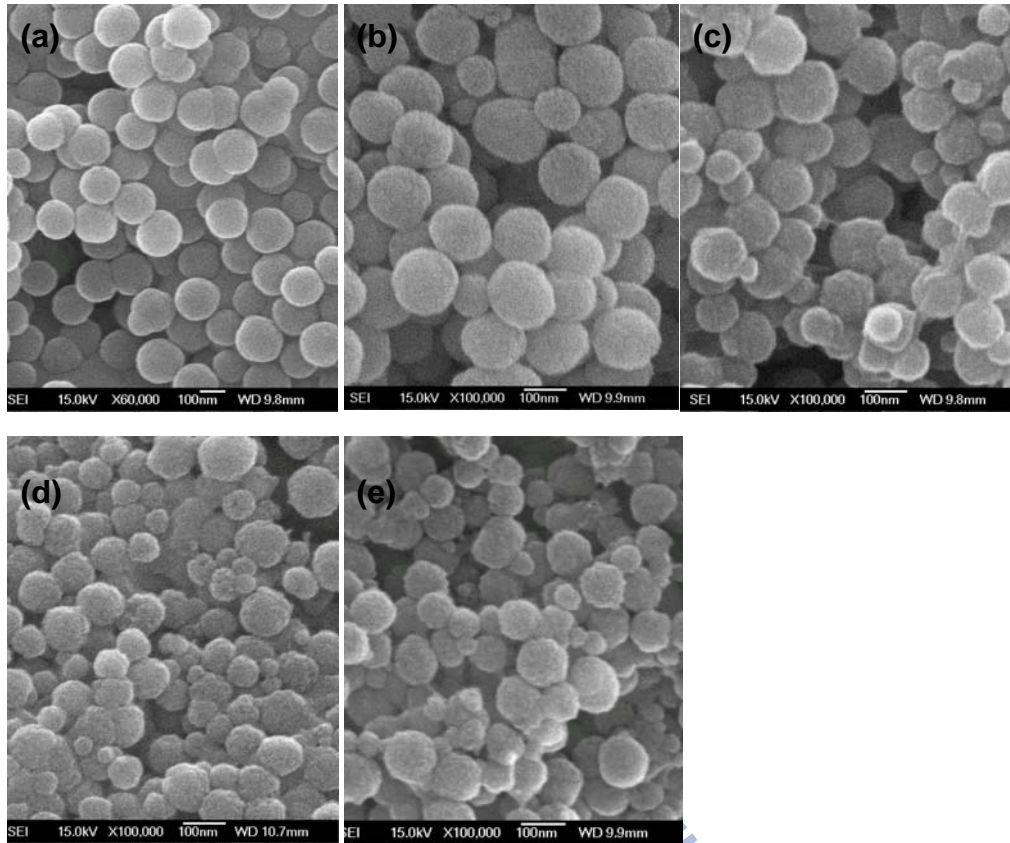units/mg particles. This result revealed that the method was enabling to trap enzyme

within.

Figure 3. SEM images of Silica-PEG-bCAT particles

(a) Silica-PEG-bCAT (10 mg) particle. (b) Silica-PEG-bCAT (30 mg) particle. (c)

Silica-PEG-bCAT (50 mg) particle. (d) Silica-PEG-bCAT (80 mg) particle. (e)

Silica-PEG-bCAT (100 mg) particle. As the SEM images show, adding proteins (Catalase

from *bovine liver*) into the reaction shows smaller particle size accompany with

morphology changes. When catalase amount increased from 10 mg to 100 mg in the

reaction, the particles became irregular and aggregated.

Figure 4. SEM images of bCAT-Ru/488-PEBBLEs particles

The generated of bCAT-Ru/488-PEBBLEs exhibited a size in a range of 100-200 nm with
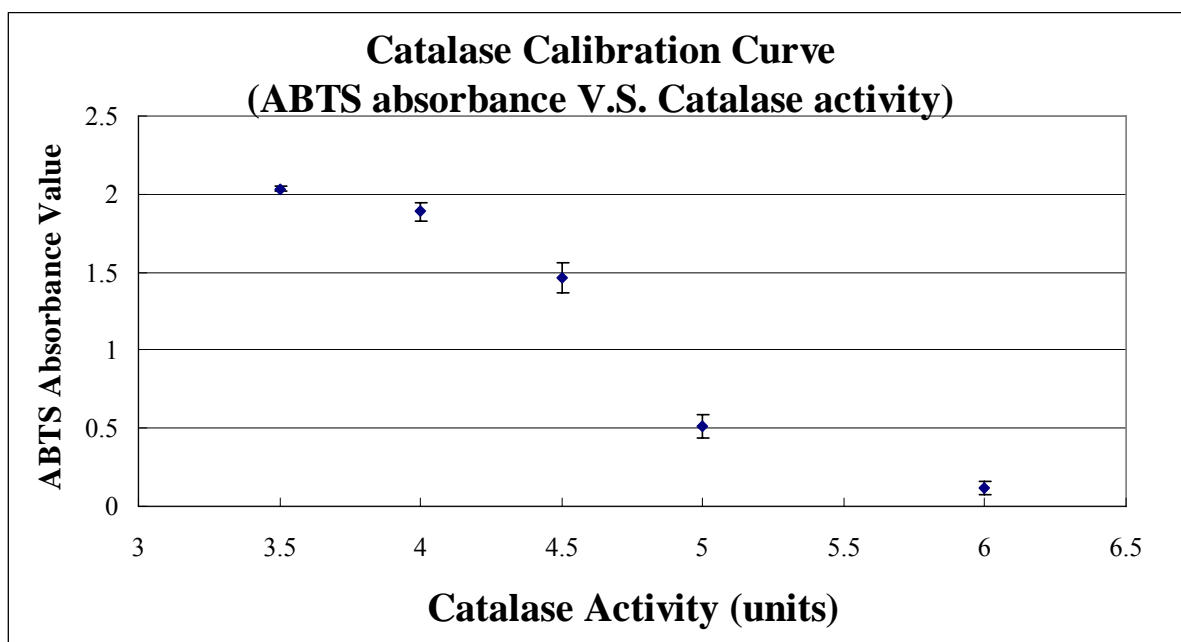
a specific activity of 0.03 units/mg particles

Figure 5. Catalase calibration curve

Catalase-HRP coupled enzyme assay was carried out to determine the activity of

bCAT-Ru/488-PEBBLE. Since PEBBLEs raises no obvious background in oxidized ABTS

solution at 405 nm, this calibration curve is suitable for activity test of

bCAT-Ru/488-PEBBLE, especially when particles with lower specific activity.
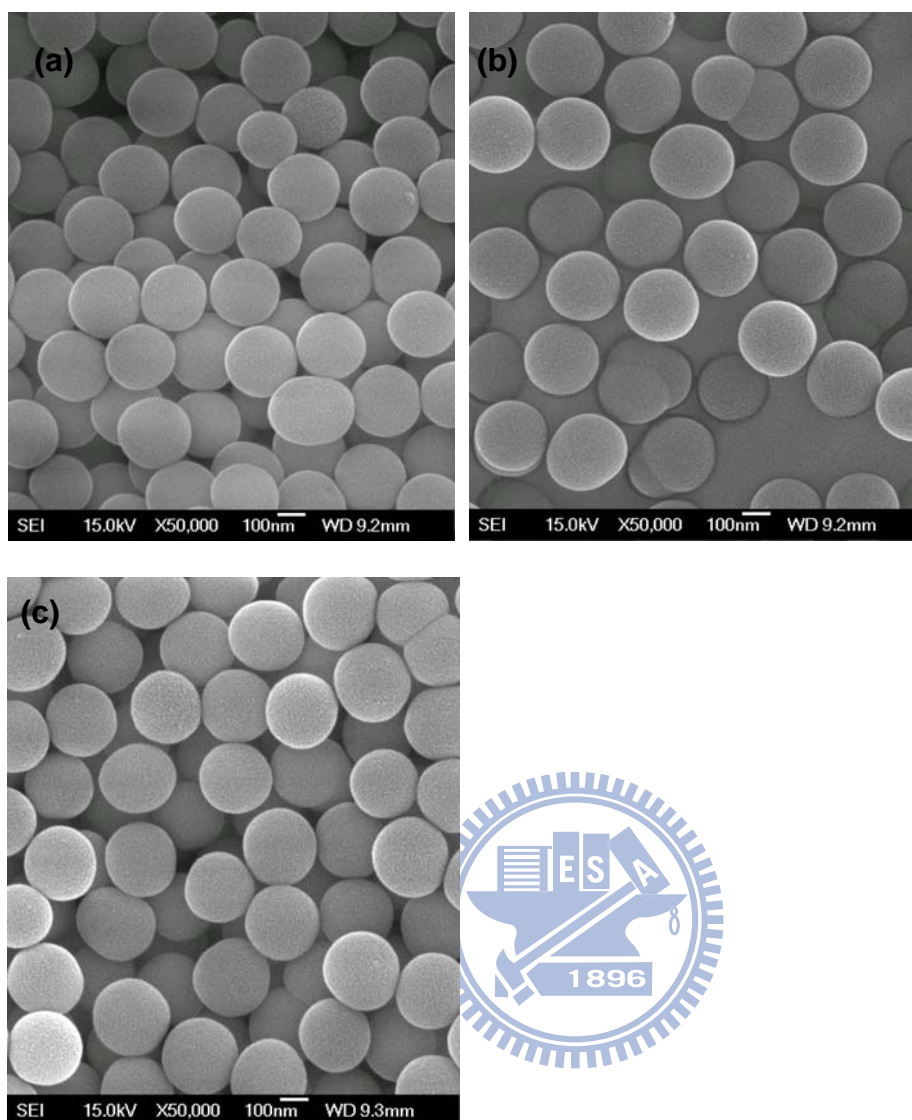
Figure 6. SEM images of Silica-PEG-cgCAT (from *Corynebacterium glutamicum*) particles

(a) Silica-PEG-cgCAT (10 μL) exhibits a particle size of 300-400 nm with a specific

activity of 20 units/mg (b) Silica-PEG-cgCAT (30μL) exhibits a particle size of 300-400

nm with a specific activity of 90 units/mg (c) Silica-PEG-cgCAT (50μL) exhibits a particle

size of 300-400 nm with a specific activity of 138units/mg. Particles are fabricated by

adding different volume of Catalase from *Corynebacterium glutamicum* (solution,

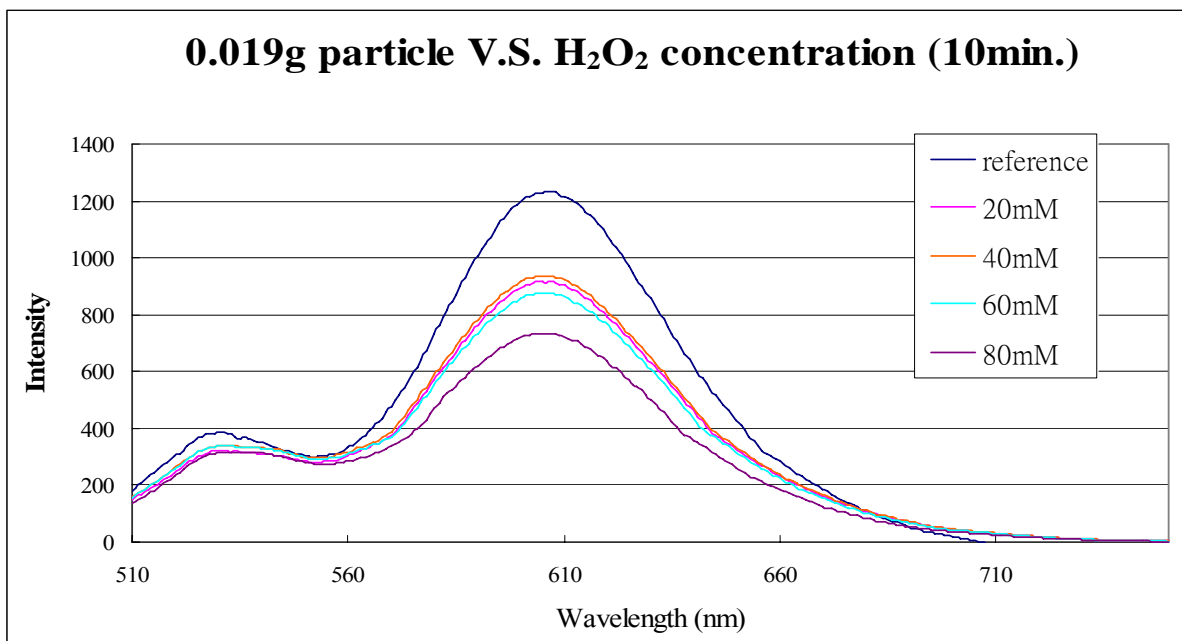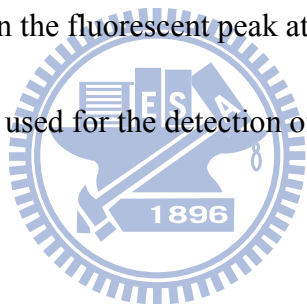1500units/μL) and fluorescence dyes. Reaction composition was summarized in Table 2.

0.019g particle V.S. H₂O₂ concentration (10min.)

Figure 7. Fluorescence emission spectrum of bCAT-Ru/488-PEBBLEs

The quenching effect of H_2O_2 on the fluorescent peak at 607 nm ($[Ru(dpp)_3]^{2+}$) indicated

that the particle was ready to be used for the detection of hydrogen peroxide.
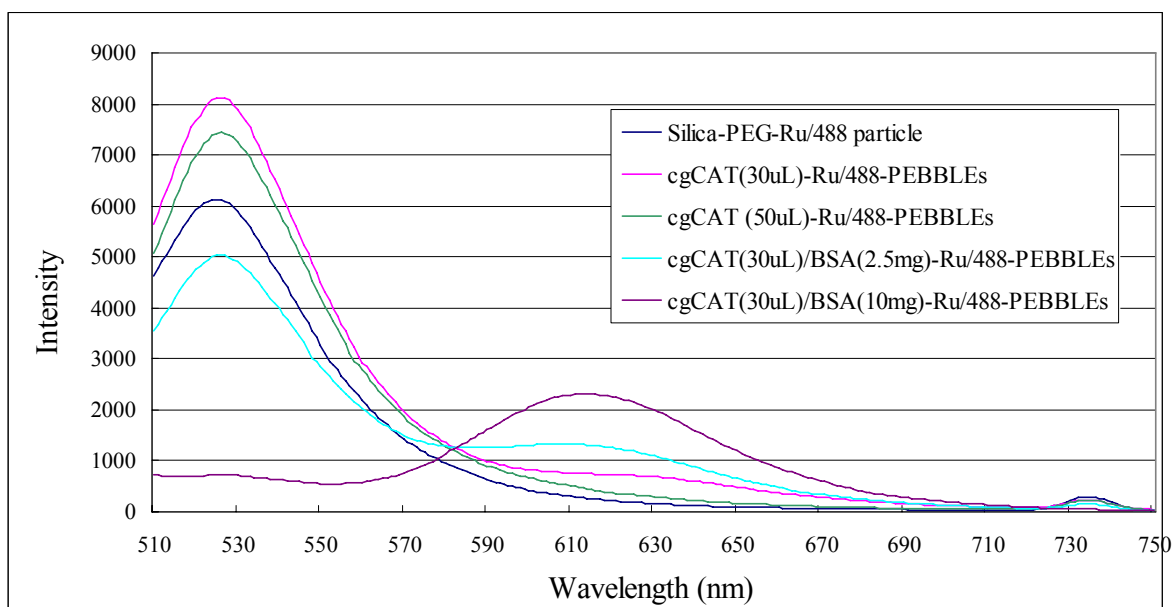
Figure 8. Fluorescence spectrum of cgCAT/BSA-Ru/488-PEBBLE v.s. [H₂O₂]

Fluorescence spectrum shows that when the ratio of catalase to BSA increased in the reaction composition, the fluorescencedye entrapping efficiency was altered. When the amount of protein increased, the intensity of fluorescent peak at 607 nm ($[Ru(dpp)_3]^{2+}$) increased, while the intensity of fluorescent peak at 524 nm (Oregon Green 488-Dextran®) decreases.
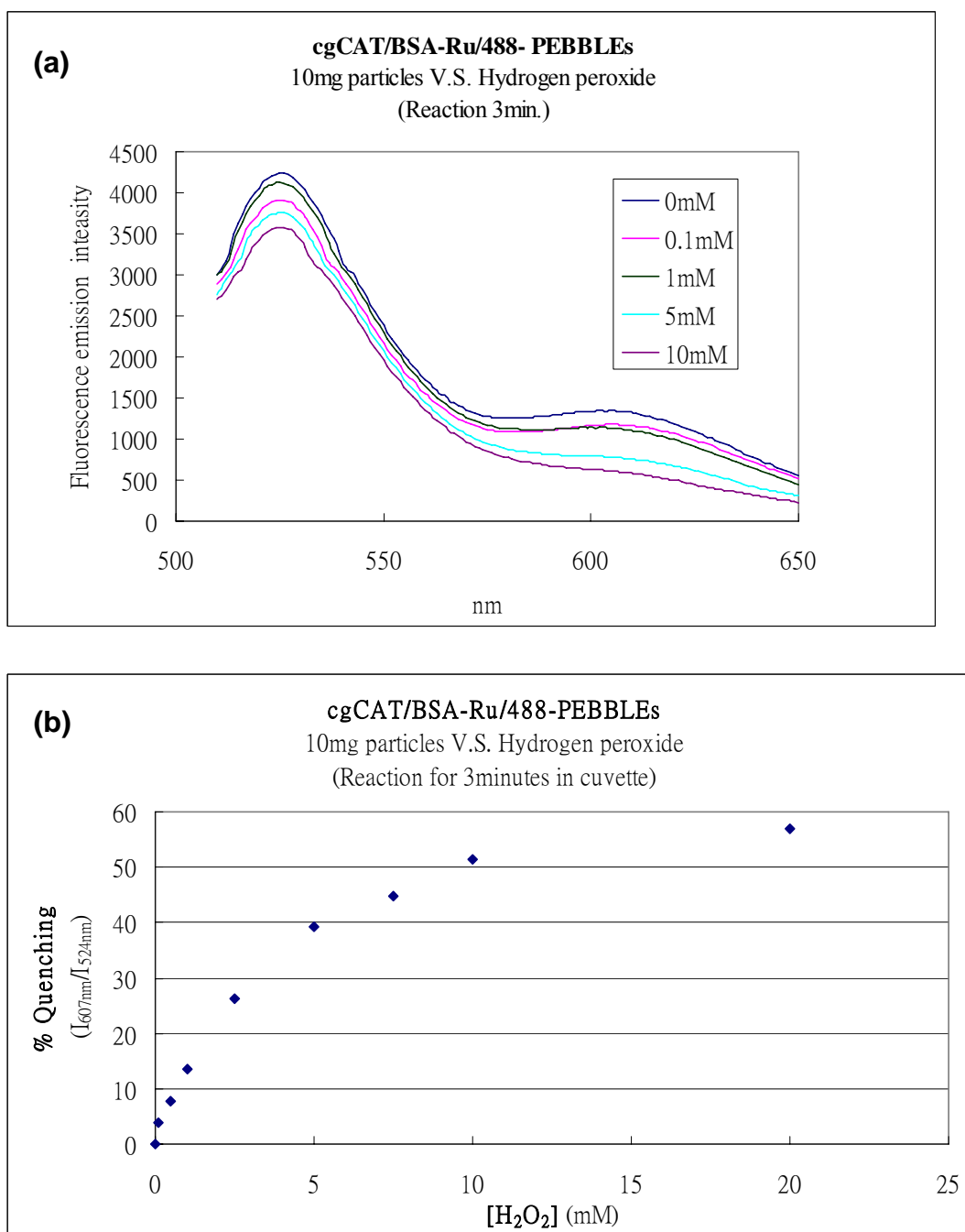
Figure 9. Fluorescence emission spectrum cgCAT/BSA-Ru/488-PEBBLEs.

(a) CAT (30μL)/BSA (2.5mg)- Ru/488-PEBBLEs v.s. [H2O2] fluorescence spectrum. The

spectrum shows that the fluorescence intensity of peak at 607 nm ($[Ru(dpp)_3]^{2+}$) was

inversely proportional to the [H_2O_2] concentration and capable to detect [H_2O_2] changes in

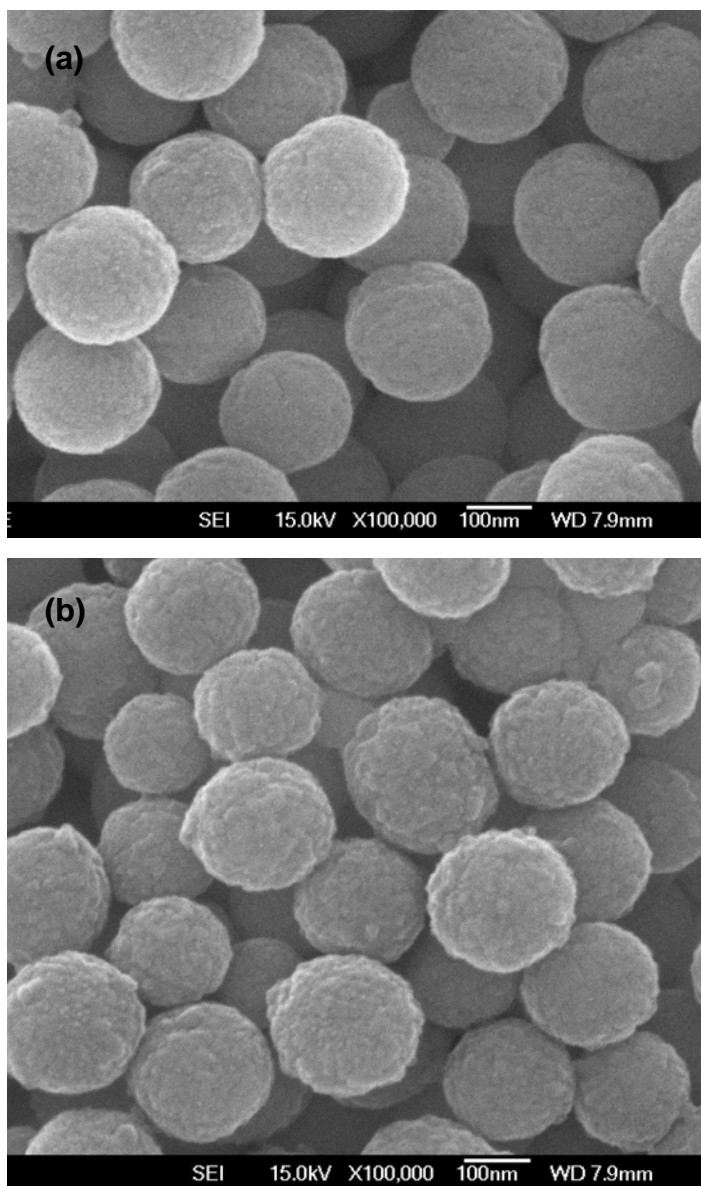the environment. (b) Normalized standard curve from data of (a).

Figure 10. SEM images of cgCAT/BSA-RU/488-PEBBLEs

 (a) The cgCAT/BSA(2.5 mg)-Ru/488-PEBBLE exhibits a particle size of 200-300 nm with a specific activity of 7.8 units/mg particles (b) The cgCAT/BSA(10 mg)-Ru/488-PEBBLE exhibits a particle size of 200-300 nm with a specific activity of <0.5 units/mg. BSA may increase $[Ru(dpp)_3]^{2+}$ entrapping efficiency. The particle prepared in the presence of 2.5mg BSA was smooth on the surface and spherical in shape. In comparison, particles prepared in the presence of 10 mg BSA, exhibited roughed surface.
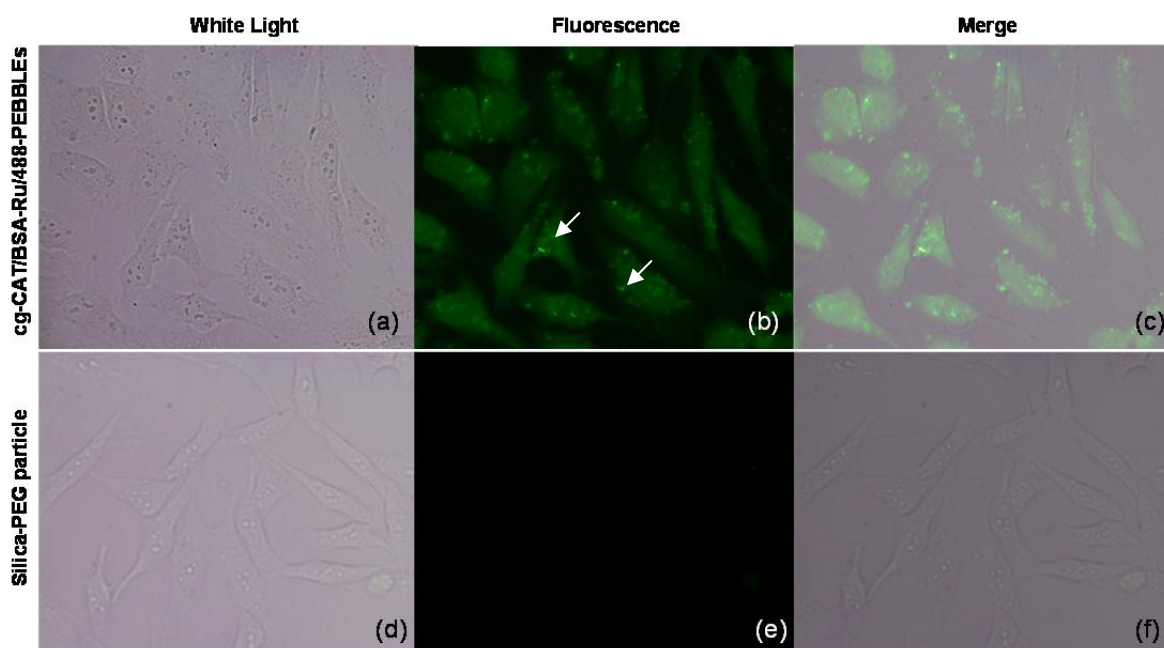
Figure 11. Fluorescent microscopy images of HeLa cell incubated with cgCAT/BSA-Ru/488-PEBBLEs

As the green fluorescence of the Oregon Green 488-Dextran[®] (524nm) showed in Figure 11b, indicated that the fluorescence signal of the cgCAT/BSA-Ru/488-PEBBLEs is successfully entrapped in the silica-PEG matrix and localized inside of the HeLa cell (as pointed by the white arrow in the figure). In contrast, Silica-PEG particle were also incubated with HeLa cell, which showed no fluorescence signals.

6. References

1. M. Valko, C.J. Rhodes, Free radicals, metals and antioxidants in oxidative stress-induced cancer *Chemico-Biological Interactions* 160, 1–40, 2006

2. T. Finkel, N.J. Holbrook, *NATURE,* Oxidants, oxidative stress and the biology of ageing, 408, 239-247, 2000

3. J. Chandra, A. Samall, S. Orrenius. Triggering and modulation of apoptosis by oxidative stress. *Free Radical Biology & Medicine*, 29, 323–333, 2000

4. B. Palmieri, V. Sblenuorio, Oxidative stress detection: what for? Part I, *European Review for Medical and Pharmacological Sciences*, 10: 291-317, 2006

5. B. Palmieri, V. Sblenuorio, Oxidative stress detection: what for? Part II, *European Review for Medical and Pharmacological Sciences*, 11: 27-54, 2007

6. M. Valko, M. Izakovic, Role of oxygen radicals in DNA damage and cancer incidence, *Molecular and Cellular Biochemistry* 266: 37–56, 2004

7. M. Valko, D. Leibfritz, Free radicals and antioxidants in normal physiological functions and human disease, *The International Journal of Biochemistry & Cell Biology*, Volume 39: 44-84, 2007

8. Enrique Cadenas, Kelvin J. A. Davies, Mitochondrial free radical generation, oxidative stress, and aging, *Free Radical Biology and Medicine*, 29: 222-230, 2000

9. Jose M. Mates, Francisca M. Sanchez-Jimenez, Role of reactive oxygen species in apoptosis: implications for cancer therapy, *The International Journal of Biochemistry & Cell Biology*, 32: 157-170, 2000

10. S. J. Stohs, D. Bagchi, Oxidative mechanisms in the toxicity of metal ions, *Free Radical Biology and Medicine*, 18: 321-336, 1995

11. F. Peter Guengerich, Common and Uncommon Cytochrome P450 Reactions Related to Metabolism and Chemical Toxicity, *Chemical Research in Toxicology* 14: 611-650, 2001

12. Lawrence J. Marnett, Oxyradicals and DNA damage, *Carcinogenesis* 21: 361-370, 2000

13. Nageswara R. Madamanchi, Aleksandr Vendrov and Marschall S. Runge, Oxidative Stress and Vascular Disease, *Arterioscler. Thromb. Vasc. Biol.* 25: 29-38, 2005

14. Kevin J. Barnham, Colin L.Masters, Ashley I. Bush, Neurodegenerative diseases and oxidative stress, *Nature Reviews Drug Discovery* 3, 205-214,2004

15. Peter Jenner, Oxidative Stress in Parkinson's Disease, *Annals of Neurology*, 53: 26-38, 2003

16. William R. Markesbery, Oxidative Stress Hypothesis in Alzheimer's Disease, *Free Radical Biology and Medicine*, 23: 134-147, 1997

17. Mark A. Smith, Catherine A. Rottkamp, Akihiko Nunomura, Arun K. Raina, George Perry, Oxidative stress in Alzheimer's disease, *Biochimica et Biophysica Acta (BBA) - Molecular Basis of Disease*, 1502: 139-144, 2000

18. J. Emerit, M. Edeas, F. Bricaire, Neurodegenerative diseases and oxidative stress, *Biomedecine & Pharmacotherapy*, 58: 39-46, 2004

19. F. Lisdat; F. W. Scheller, Principles of Sensorial Radical Detection-A Minireview, *Analytical Letters*, 33: 1-16, 2000

20. Margaret M. Tarpey, David A. Wink and Matthew B. Grisham, Methods for detection of reactive metabolites of oxygen and nitrogen: in vitro and in vivo considerations, *Am J Physiol Regulatory Integrative Comp Physiol*, 286: 431-444, 2004.

21. Ana Gomes, Eduarda Fernandes, Jose L.F.C. Lima, Fluorescence probes used for detection of reactive oxygen species, *Journal of Biochemical and Biophysical Methods*, 65: 45-80, 2005

22. Kelley A. Foster, Francesca Galeffi, Florian J. Gerich, Dennis A. Turner, Michael Muller, Optical and pharmacological tools to investigate the role of mitochondria during oxidative stress and neurodegeneration, *Progress in Neurobiology*, 79:

136-171, 2006

23. James F. Curtin, Maryanne Donovan, Thomas G. Cotter, Regulation and measurement of oxidative stress in apoptosis, *Journal of Immunological Methods*, 265: 49-72, 2002

24. Dongwon Lee, Sirajud Khaja, Juan C. Velasquez-Castano, Madhuri Dasari, Carrie Sun, John Petros, W. Robert Taylor, Niren Murthy, *In vivo* imaging of hydrogen peroxide with chemiluminescent nanoparticles, *Nature Materials* 6: 765-769, 2007

25. Yi Luo, Yun-xia Sui, Xiao-rong Wang, Yuan Tian, 2-chlorophenol induced hydroxyl radical production in mitochondria in Carassius auratus and oxidative stress - An electron paramagnetic resonance study, *Chemosphere*, 71: 1260-1268, 2008

26. Won Hyuk Suh, Kenneth S. Suslick, Galen D. Stucky, Yoo-Hun Suh, Nanotechnology, nanotoxicology, and neuroscience, *Progress in Neurobiology*, 87: 133-170, 2009

27. Kewal K. Jain, The role of nanobiotechnology in drug discovery, *Drug Discovery Today*, 10: 1435-1442, 2005

28. Dietmar Knopp, Dianping Tang, Reinhard Niessner, Review: Bioanalytical applications of biomolecule-functionalized nanometer-sized doped silica particles, *Analytica Chimica Acta*, 647: 14-30, 2009

29. OV Salata, Applications of nanoparticles in biology and medicine, *Journal of Nanobiotechnology*, 2, 2004

30. Weisheng Lin, Yue-wern Huang, Xiao-Dong Zhou, Yinfa Ma, In vitro toxicity of silica nanoparticles in human lung cancer cells, *Toxicology and Applied Pharmacology*, 217: 252-259, 2006

31. Igor I. Slowing, Brian G. Trewyn, Supratim Giri, and Victor S.-Y. Lin, Mesoporous Silica Nanoparticles for Drug Delivery and Biosensing Applications, *Adv. Funct. Mater.* 17: 1225–1236, 2007

32. David Avnir, Sergei Braun, Ovadia Lev, and Michael Ottolenghi, Enzymes and Other Proteins Entrapped in Sol-Gel Materials, *Chem. Mater.*, 6: 1605-1614, 1994

33. Minjung Cho,Wan-Seob Cho, Mina Choi, Sueng Jun Kim, Beom Seok Han, The impact of size on tissue distribution and elimination by single intravenous injection of silica nanoparticles. *Toxicol. Lett*. 2009, doi:10.1016/j.toxlet.2009.04.017 (article in express)

34. Stöber W, Fink A, Bohn E, Controlled growth of mono-disperse silica spheres in the micron size range. *J. Colloid Interface Sci.* 26:62–69,1968

35. Larry L. Hench, and Jon K. West, The sol-gel process, Chem. Rev., 90: 33-72, 1990

36. Iqbal Gill, Antonio Ballesteros, Bioencapsulation within synthetic polymers (Part 1): sol-gel encapsulated biologicals, *Trends in Biotechnology*, 18: 282-296, 2000

37. Jie Lin, Chris W. Brown, Sol-gel glass as a matrix for chemical and biochemical sensing, *Trends in Analytical Chemistry*, 16: 200-211, 1997

38. David Avnir, Thibaud Coradin, Ovadia Levc , Jacques Livage, Recent bio-applications of sol–gel materials, *J. Mater. Chem*., 16: 1013–1030, 2006

39. Wen Jin and, John D. Brennan, Properties and applications of proteins encapsulated within sol-gel derived materials, *Analytica Chimica Acta*, 461: 1-36, 2002

40. Hao Xu, Jonathan W. Aylottb and Raoul Kopelman, Fluorescent nano-PEBBLE sensors designed for intracellular glucose imaging, *Analyst*, 127: 1471-1477, 2002

41. Heather A. Clark, Susan L. R. Barker, Murphy Brasuel, Michael T. Miller, Eric Monson, Steve Parus, Zhong-You Shi, Antonius Song, Subcellular optochemical nanobiosensors: probes encapsulated by biologically localised embedding (PEBBLEs), *Sensors and Actuators B: Chemical*, 51: 12-16,1998

42. M.N. Velasco-Garcia, Optical biosensors for probing at the cellular level: A review of recent progress and future prospects, Seminars in Cell & Developmental Biology , *A Special Edition on Biosensors and Development of Pigment Cells and Pigment*

Patterns, 20: 27-33, 2009

43. Sarah M Buck, Yong-Eun Lee Koo, Ed Park, Hao Xu, Martin A Philbert, Murphy A Brasuel, Raoul Kopelman, Optochemical nanosensor PEBBLEs: photonic explorers for bioanalysis with biologically localized embedding, *Current Opinion in Chemical Biology*, 8: 540-546, 2004

44. Heather A. Clark, Marion Hoyer, Martin A. Philbert, and Raoul Kopelman, Optical Nanosensors for Chemical Analysis inside Single Living Cells. 1. Fabrication, Characterization, and Methods for Intracellular Delivery of PEBBLE Sensors, *Analytical Chemistry*, 71: 4831-4836, 1999

45. Brasuel M, Kopelman R, Miller TJ, Tjalkens R, Philbert MA: Fluorescent nanosensors for intracellular chemical analysis: decyl methacrylate liquid polymer matrix and ion exchange-based potassium PEBBLE sensors with real-time application to viable rat C6 glioma cells. *Anal Chem.*, 73: 2221-2228, 2001

46. Hao Xu, Jonathan W. Aylott, Raoul Kopelman, Terry J. Miller, and Martin A. Philbert, A Real-Time Ratiometric Method for the Determination of Molecular Oxygen Inside Living Cells Using Sol-Gel-Based Spherical Optical Nanosensors with Applications to Rat C6 Glioma, *Analytical Chemistry*, 73: 4124-4133, 2001

47. Yong-Eun Lee Koo, Youfu Cao, Raoul Kopelman, Sang Man Koo, Murphy Brasuel, and Martin A. Philbert, Real-Time Measurements of Dissolved Oxygen Inside Live Cells by Organically Modified Silicate Fluorescent Nanosensors, *Analytical Chemistry*, 76: 2498-2505, 2004

48. James P. Sumner, Nissa M. Westerberg, Andrea K. Stoddard, Carol A. Fierke, Raoul Kopelman, Cu^+- and Cu^{2+}-sensitive PEBBLE fluorescent nanosensors using DsRed as the recognition element, *Sensors and Actuators B* 113:760-767, 2006

49. Jonathan W.Aylott, Optical nanosensors—an enabling technology for intracellular measurements, *Analyst*, 128: 309-312, 2003

50. Julian S. SHINDLER, Robert E. CHILDS, and William G. BARDSLEY, Peroxidase from Human Cervical Mucus: The Isolation and Characterisation, *Eur. J. Biochem.* 65*: 325-331, 1976

51. Zhenkun Zhang, Anne E. Berns, Sabine Willbold, Johan Buitenhuis, Synthesis of poly(ethylene glycol) (PEG)-grafted colloidal silica particles with improved stability in aqueous solvents, *Journal of Colloid and Interface Science*, 310: 46-455, 2007

52. Hao Xu, Fei Yan, Eric E. Monson, Raoul Kopelman, Room-temperature preparation and characterization of poly(ethylene glycol)-coated silica nanoparticles for biomedical applications, *Journal of Biomedical Materials Research. Part A*, 66: 870 -879, 2003

53. A. G. A. Coombes, S. Tasker, M. Lindblad, J. Holmgren, K. Hoste, V. Toncheva, E. Schacht, M. C. Davies, L. Illum, S. S. Davis, Biodegradable polymeric microparticles for drug delivery and vaccine formulation: the surface attachment of hydrophilic species using the concept of poly(ethylene glycol) anchoring segments, *Biomaterials*, 18: 1153-1161, 1997

54. Magdalena Prokopowicz, Silica-Polyethylene Glycol Matrix Synthesis by Sol-Gel Method and Evaluation for Diclofenac Diethyloammonium Release ,*Drug Delivery*,14: 129-138, 2007

55. Alpa C. Patel, Shuxi Li, Jian-Min Yuan, and Yen Wei, In Situ Encapsulation of Horseradish Peroxidase in Electrospun Porous Silica Fibers for Potential Biosensor Applications, *Nano Lett.*, 6: 1042–1046, 2006

56. Ekaterina N. Kadnikova, Nenad M. Kostic, Oxidation of ABTS by hydrogen peroxide catalyzed by horseradish peroxidase encapsulated into sol-gel glass.: Effects of glass matrix on reactivity, *Journal of Molecular Catalysis B: Enzymatic*, 18: 39-48, 2002

57. Mark Alston, Andy Willetts, Andy Wells, Polymer-Supported Catalase: A Green Approach to the Removal of Hydrogen Peroxide from Reaction Mixtures, *Org. Proc.*

Res. Dev., 6: 505-508, 2002

58. Roche Applied Science, *Microbial Catalase for Industry*, 3. ed., May 2006

59. Silgia A. Costa, Tzanko Tzanov, Ana Filipa Carneiro, Andreas Paar, Georg M. Gubitz, Artur Cavaco-Paulo, Studies of stabilization of native catalase using additives, *Enzyme and Microbial Technology*, 30: 387-391, 2002

60. John D. Mackenzie and Eric P. Bescher, Chemical Routes in the Synthesis of Nanomaterials Using the Sol–Gel Process, *Acc. Chem. Res.*, 40: 810–818, 2007

61. Iqbal Gill, Bio-doped Nanocomposite Polymers: Sol−Gel Bioencapsulates, *Chem. Mater.*, 13: 3404–3421, 2001

62. Dorota Napierska, Leen C. J. Thomassen, Virginie Rabolli, Dominique Lison,Laetitia Gonzalez, Micheline Kirsch-Volders, Johan A. Martens, and Peter H. Hoet, Size-dependent cytotoxicity of monodisperse silica nanoparticles in human endothelial cells, *Small*, 5: 846–853, 2009